DIPLOMA THESIS

Experimental Investigation of the Systematic Errors of Pneumatic Pressure Probes Induced by Velocity Gradients

written at
Institute of Thermal Turbomachines and Powerplants
Vienna University of Technology

under direction of
O. Univ. Prof. Dipl.-Ing. Dr. techn. H. HASELBACHER
and
Univ. Ass. Dipl.-Ing. Dr.techn R.WILLINGER

by
Eduardo SEVILLA
Pfeilgasse 3A
A-1080 Vienna

Vienna, September 2002

Abstract

Pneumatic pressure probes are a reliable and robust tool for flow measurement in components of thermal turbomachines. Three-hole probes are used for two dimensional flow fields and five-hole probes for three-dimensional flow fields, respectively. The calibration of the probes is usually performed in a free-jet wind tunnel with constant velocity. However, the flow field downstream of turbomachinery blade rows shows considerable gradients of pressure and velocity. Therefore, systematic errors in the measured quantities -especially in the flow angle- occur.
The present diploma thesis is a investigation on the influence of velocity gradients on the flow angle error of pneumatic three-hole probes. The work starts with a literature survey on this topic. The next step is the calibration of the three-hole probe in a flow field of constant velocity magnitude. The hole and calibration coefficients are compared with results obtained from the simple streamline projection method. This method is also used for an estimation of the principle effect of velocity gradients. The strength of the gradient can be described by a nondimensional velocity gradient K and the flow angle error $\Delta\varepsilon$ is proportional to K.

The appropriate constant is determined experimentally. A natural turbulent boundary layer is used for this investigation. The velocity distribution is measured with a single hot-wire probe and the three-hole probe is traversed in the boundary layer

Finally, the correction method is applied to the measured flow field downstream of a linear turbine cascade. An appreciate improvement of the measured flow angle distribution is achieved by the application of the correction method.

1 Table of Contents

2 List of Symbols

a_{23}	[m(mm)]	Distance between hole 2 und hole 3
C	[1]	Constant
d	[m(mm)]	Thickness of the three-hole probe
d_h	[m(mm)]	Diameter of the probe hole
k_i	[1]	Hole coefficients (i=1,2,3)
$\bar{k}$	[1]	Coefficient defined by Equ. 33
K	[1]	Nodimensional velocity gradient
k_s	[1]	Static pressure coefficient
k_s'	[1]	Static pressure experimental coefficient
k_t	[1]	Total pressure coefficient
k_t'	[1]	Total pressure experimental coefficient
k_β	[1]	Directional coefficient (yaw plane)
k_β'	[1]	Directional experimental coefficient (yaw plane)
k_γ	[1]	Directional coefficient (pitch plane)
k_γ'	[1]	Directional experimental coefficient (pitch plane)
k_1	[1]	Hole coefficient 1
k_2	[1]	Hole coefficient 2
k_3	[1]	Hole coefficient 3
Ma	[1]	Mach number
n	[1]	Constant in the power law
p	[Pa(N/m^2)]	Static pressure
$\bar{p}$	[Pa(N/m^2)]	Mean Pressure defined by Equ. 5
p_{ref}	[Pa(N/m^2)]	Pressure reference
p_t	[Pa(N/m^2)]	Total pressure
p_1	[Pa(N/m^2)]	Static pressures measured at the central probe hole
p_2, p_3	[Pa(N/m^2)]	Static pressures measured in the yaw plane
p_4, p_5	[Pa(N/m^2)]	Static pressures measured in the pitch plane
q	[Pa(N/m^2)]	P_t-p
r	[m(mm)]	Radius
Re	[1]	Reynolds number

t	[C]	Temperature
Tu	[%]	Turbulence intensity
w	[m/s]	Velocity
w_∞	[m/s]	Free stream velocity
y	[m(mm)]	Distance
α_i	[1]	Hole coefficients for turbulence (i=1,2,3,4,5)
Δw	[m/s]	Difference velocity between hole 2 und hole 3
Δy	[m(mm)]	Distance (interval)
$\Delta\beta$	[deg[°]]	Relative flow angle (yaw-plane)
$\Delta\beta'$	[deg[°]]	Experimental relative flow angle (yaw-plane)
$\Delta\gamma$	[deg[°]]	Relative flow angle (pitch-plane)
$\Delta\gamma'$	[deg[°]]	Experimental relative flow angle (pitch-plane)
$\Delta\varepsilon$	[deg[°]]	Error of the flow angle
δ	[deg[°]]	Probe wedge angle
δ	[m(mm)]	Displacement of probe measuring point
η	[m(mm)]	Boundary layer thickness
ν	[m^2/s]	Kinematic viscosity
ρ	[kg/m^3]	Fluid mass density

3 Introduction

Pneumatic pressure probes are a reliable and robust tool for flow measurements in components of thermal turbomachines. The pressures measured at the probe sensing holes are used for the estimation of the velocity in an indirect manner. Prior to the measurement in the turbomachine, the probe has to be calibrated regarding the magnitude and the direction of the flow. An open jet wind tunnel is used for this calibration task. The pressure probe is positioned at a number of predefined angular settings in a free jet with constant velocity magnitude and low turbulence intensity. After the calibration task, nondimensional coefficients (calibration coefficients) will be derived from the measured pressures at the probe sensing holes.

The flow field downstream of a turbomachinery blade row differs considerably from the flow field in the free jet. The former is characterized by strong spatial gradients of static pressure as well as velocity. In contrast, the free jet shows constant static pressure and velocity magnitude. This results in systematic measurement errors of the measured flow direction downstream of the blade row. The error is mainly induced by the velocity gradients. For three-and five-hole pressure probes, the error is proportional to the velocity gradient and to the characteristic length scale of the probe head.

The scope of the present work is the investigation of the influence of velocity gradients on the measurement results of pneumatic pressure probes. Special attention should be paid on three-hole pressure probes. As a starting point the appropriate results in the available literature should be ordered and summarized. The main topic of the work is the planning, execution and evaluation of experiments in the linear cascade wind tunnel of the institute. The wind tunnel has to be adapted for this kind of experiments. The turbulent end wall boundary layer developing in the wind tunnel duct acts as a flow field with predefined velocity gradients. A hot-wire probe should be used for the velocity and turbulence measurements in the boundary layer. The results of the experimental investigation should supply the framework for a

modification of the currently used computer programs. The programs are used for the evaluation of three-hole and five-hole probe measurements downstream of turbomachinery blade rows.

4 Three Hole Pressure Probe

4.1 Geometry

The three-hole pressure probe used in this investigation is shown in Fig. 1. The dimension of the probe head are 0,8 × 2,4 mm with forward facing tubes. The total cone angle is 60° and the diameter of the probe stem in 6 mm, respectively.

The nomenclature used for the three-hole probe is shown in Fig. 2. The characteristic dimension of the probe head is d. Hole 1 is the centre hole and the holes 2 and 3 are separated by the dimension a_{23}. The relative flow angle $\Delta\beta$ is measured between the centre line of the probe head and the flow direction, whereas the magnitude of the velocity is denoted w.

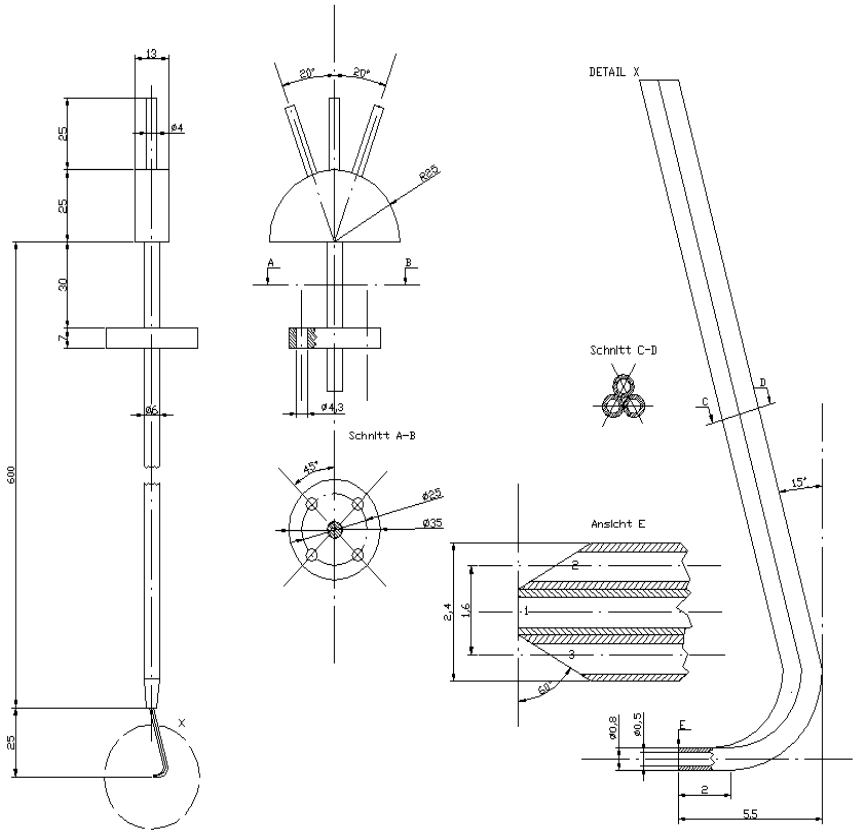

Fig. 1: Three-hole pressure probe used for the investigation

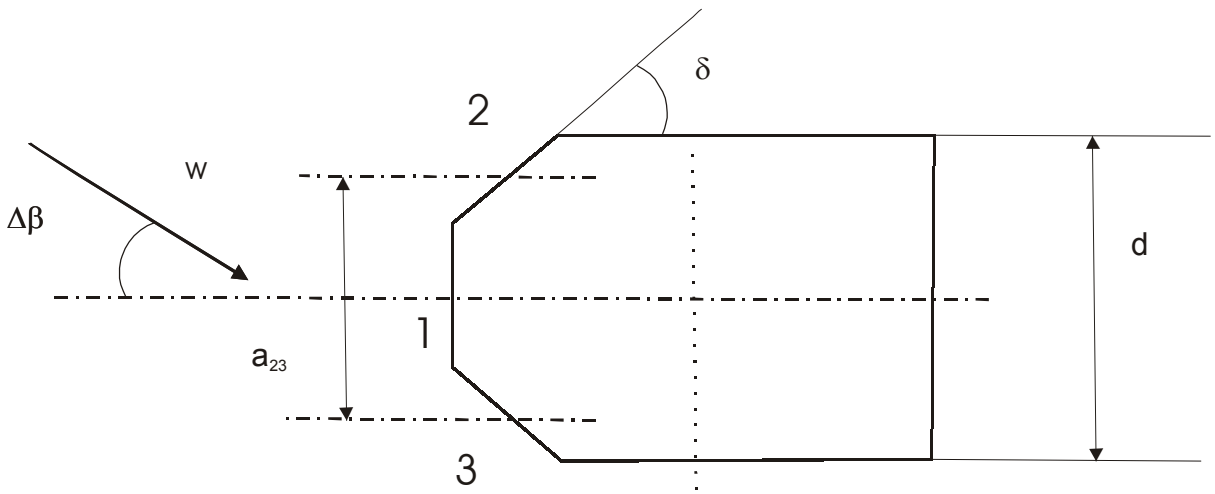

Fig. 2: Nomenclature used for the three-hole probe

4.2 Calibration

In many complex flow fields such as those encountered in turbomachines, the experimental determination of the steady-state, three-dimensional characteristic of the flow field are frequently required. If space limitations or other considerations make nulling techniques impractical, three-hole probes in a non-mulling mode can be employed. However, this application requires complete two dimensional calibration data which are not usually supplied by commercial vendors.

The three-hole probe employed in this study is used in a fixed position or non-nulling mode. This means that relationships must be determined between the measured pressures at the three holes and the true, local total and static pressure as well as the flow direction. These derived relationships are usually expressed in dimensionless pressure coefficients, which are functions of flow angularity. The whole process of the investigation of the dimensionless pressures coefficients is called calibration. It would be advantageous if the calibration characteristics of a three-hole probe could be determined by analytical procedures. However, due to manufacturing inaccuracies, an experimental calibration is required for pneumatic pressure probes. Furthermore, the complex geometries characterized by abrupt

changes in contour are subject to flow separation and viscous effects which can not be modelled by analytical procedures or computational fluid dynamics.

The calibration of the three-hole probe is performed in a free jet wind tunnel with constant velocity, as will be described later in this report.

4.3 Errors

The flow field downstream of a turbomachinery blade cascade is different from the flow field in the free jet wind tunnel used for the calibration. Therefore, a number of sources of systematic errors occur .

- Reynolds number
- Mach number
- Turbulence intensity
- Velocity gradient
- Wall proximity effects
- Blockage effects of probe and stem
- Probe vibration
- Fouling of the sensing holes.

The present work focuses on the influence of velocity gradients on the measured flow angle of a three-hole probe.

5 Literature

The work of Treaster and Yocum [10] focuses mainly on five-hole probes. However, their results are also useful for three-hole probes.

In many complex flow fields such as those encountered in turbomachines, the experimental determination of the steady-state, three dimensional characteristics of the flow field are frequently required. If space limitations or other considerations make nulling techniques impractical, five-hole probes in a non-nulling mode can be employed. However, this application requires complete three-dimensional calibration data which are not usually supplied by commercial vendors. The resultants of programs to calibrate and employ five-hole probes of both angle-tube and prismatic geometries are presented in this introduction. Descriptions of the calibration technique, typical calibration data, and an accompanying discussion of the application or interpolation procedure are included. Also, the variations in the calibration data due to Reynolds number and wall proximity effects are documented in this project. Typical measured data are included and, where applicable, these data are validated by comparision with data obtained using other types of instrumentation.

. Thus, the measurement of these data and the development of an interpolation procedure become the responsibility of the user.

The application of five-hole probes is not new but rather it dates back as far as Admiral Taylor´s work in 1915. Other work followed; but Pien was the first to show theoretically that for a spherical probe the velocity component in any plane in space can be obtained independently from three pressure measurements in that plane. Although this potential flow solutions is valid for perfectly formed spherical probes in inviscid flows of restricted angularity Pien found it necessary to obtain experimental calibration data. More recently, the work of Hurwitz and Dick has indicated the need to individually calibrate each probe. The initial program employing five-hole probes involved the measurement of the three-dimensional wake in the propeller plane of surface ship model installed in the test section of the 48-in. dia water tunnel. Since the probes to be employed were of angle tube and prismatic geometries, the approach of Krause and Dudzinski which includes geometric and viscous effects,

was most applicable. However, this method required extension to enable the measurement of the local pressures and the magnitude and direction of the corresponding velocity at the probe tip.

Because the goals of the five-hole probe program were application-oriented, the objectives of the five-hole probe phase of the program were rather pragmatic in nature. Primary objectives were specified in three areas : (1) calibration, to develop the necessary hardware and experimental procedures to use existing test facilities for the calibration of the five-hole probes; (2) analysis, to develop interpolation and data reduction procedures that use the calibration data and the measured pressures to define the velocity vector at the probe tip; and (3) measurement, to survey known and unknown three-dimensional flow fields.

Because calibration data should be independent of measured quantities, the effects of Reynolds number variations were assessed by calibrating the prism probe in air over a Reynolds number range of 2000 to 7000. The angle-tube probes were calibrated in water at a Reynolds number of 20000 and in air at 8400. The effect of wall proximity on the calibration characteristics was also investigated. Both types of probes have been used in subsequent programs; characteristic results are included.

As the name implies, five-hole probes are characterized by five pressure-sensing hole lying in two perpendicular planes with the line of intersection of the two planes passing through the central hole. Two different hole arrangements exist.

Five-hole, probes are commercially available in several configurations, such as spherical, conical, prismatic, etc. The primary emphasis in this paper will be placed on the results obtained while using the commercially available (0,318-cm) dia prism probe and the angle-tube probe. The angle-tube probes were fabricated at according to the criteria presented in references. The probe tip was made from five pieces of (0,127-cm) dia hypodermic tubing, which had an assembled diameter of (0,381-cm). The tubes were bonded together with soft solder. Tangential epoxy fillets between the tubes were hand-formed to acceptable hydrodynamic contours. A (0,635-cm) dia supporting member of circular cross section was chosen to avoid possible angle of attack errors, which may be introduced with a more stream lined shape. The probe tip

was located four support diameters upstream of this member to avoid support interference effects. The support was extended four support diameters beyond the tubing to improve the flow symmetry at the probe tip.

The geometry of the prism probe facilitates its use in turbomachinery research, since it can be easily inserted through casings and used in studies where spatial restrictions are present. The geometry of the angle-tube probes has generally limited their use to studies where the presence of flow boundaries has not been a problem.

Calibration for five-hole probe

The five-hole probes employed in this study were used in a fixed position or non-nulling mode. This means that relationships must be determined between the measured pressures at the five hole and the true, local total and static pressure or velocity. These desired relationships are usually expressed as dimensionless pressure coefficients, which are functions of the flow angularity. Since, when in use, the flow angles are unknown, relationship between the five measured probe pressures and the flow direction are also required.

It would be advantageous if the calibration characteristics of a five-hole probe could be determined by analytical procedures. For probes of spherical geometry, a potential flow solution can predict the pressure distribution and the corresponding calibration characteristics to a reasonable accuracy. However, due to manufacturing inaccuracies and to operating range and accuracy requirements encountered in the laboratory or field conditions, calibrations are required for probes of this simple geometry. For probes of angle-tube or prismatic geometry, analytical procedures of any type are difficult. These complex geometries, characterized by abrupt changes in contour, are subject to flow separation and viscous effects that are not modelled by current computational techniques. Thus the only mathematical consideration at this stage is how to represent a given probe´s response characteristics to a known flow field.

For operation in the non-nulling mode, it is apparent that the calibration characteristics must include data that represent pressure differences in both the pitch

and yaw planes. As well as differences between the measured and the true, local total and static pressures. The pressure coefficients representing these data must be defined so that they are independent of velocity and are a function only of the flow angularity. Krause and Dudzinski found that an indicated dynamic pressure formed by the difference between the indicate total pressure p_1 and the averaged value of the four indicated static pressures, p_2, p_3, p_4, and p_5, was a satisfactory normalizing parameter. It was demonstrated that this normalizing parameter reduced the scatter in the calibration data as compared to using the true dynamic pressure. This is convenient, since using the true dynamic pressure would have introduced an unknown quantity. The four calibration coefficients are defined as follows:

$$k_\beta = (p_2 - p_3)/(p_1 - \overline{p})$$

Equ. 1

$$k_\gamma = (p_4 - p_5)/(p_1 - \overline{p})$$

Equ. 2

$$k_t = (p_1 - p_t)/(p_1 - \overline{p})$$

Equ. 3

$$k_s = (\overline{p} - p)/(p_1 - \overline{p})$$

Equ. 4

$$\overline{p} = (p_2 + p_3 + p_4 + p_5)/4$$

Equ. 5

The pitch and yaw planes are inclined by 90 degree. Their orientation relative to the probe is dependent on the device used to position the probes during calibration. The “yaw-pitch” device was used in a uniform flow field and permitted first a rotation of the probe about its longitudinal axis, i.e a change in yaw angle $\Delta\beta$. The probe was then tilted forward or backward providing a change in pitch angle $\Delta\gamma$.

An alternate approach would be to use a “pitch-yaw” device which permitted a pitching motion followed by a yawing motion. Either approach is satisfactory if the user is consistent in the resolution of the velocity vectors. For both calibration and application the probe´s reference line is defined by some consistent characteristic of the probe geometry. In application, a reference direction obtained by balancing , p_2, with p_3, and p_4, with p_5 is not always meaningful, since initially a known flow direction would be required to relate the balanced condition to an absolute spatial reference.

The previously discussed yaw-pitch calibration device, which is installed in the circular test section of the 12-in. dia water tunnel permitted a ±30 deg rotation in both pitch and yaw. Because uniform flow fields were available in the 12-in. dia water tunnel and in the open-jet facility, a more complex device that would have maintained the probe tip at a fixed location was not required.. During the calibrations conducted in the open-jet facility, precautions were taken to insure that the probes were located in the potential core of the jet. The velocity in the test section of the water tunnel and in the potential core of the jet had been shown by previous studies to be uniform within the accuracy of the experimental measurements.

The reference total pressure was measured in the upstream settling section, and atmospheric pressure was used as the reference static pressure. A similar arrangement was used in the water tunnel calibrations, except that the reference static pressure was recorded by wall-pressure taps in the test section.

To conduct the calibration of a given probe, the test velocity was maintained at a constant value. For calibrations conducted in the 12-in. dia water tunnel, the test section pressure was set at a value that was high enough to avoid cavitation at the probe tip. The probe was positioned at one of the predetermined yaw angles and then moved prescribed increments through the pitch angle range. At each of the calibration points, the seven differential pressures are measured. The data reduction program enabled the calculation of the four previously defined pressure coefficients, the test section velocity and the Reynolds number based on the probe tip diameter. Each probe was calibrated three times to verify the repeatability of the resultants. To reduce deviations in the calibration data, the results were averaged.

Analysis of the calibration

Basically, the calibration data for the two probes are similar; the differences can be primarily attributed to geometric characteristics. One difference is indicated by the comparison of the k_γ vs k_β grids, which show that the prism probe has a much smaller range of k_γ values. This reduced range will result in an increased sensitive of the prism probe to small flow variations in the pitch plane. The velocity component in this plane may, therefore, exhibit more data scatter.

The smaller range in k_γ is attributed to the different tips of surface on which the holes in the two planes are located. At large yaw angles, one hole in the yaw planes is approximately aligned with the flow and senses pressure near the free-stream total pressure. The other hole senses a pressure much less than the free-stream static pressure, due to the acceleration of the flow around the probe and possibly due to flow separation. For the prism probe, however, the holes in the pitch plane have a different response. At large pitch angles, one hole again senses a pressure near the free-stream, total pressure, whereas the other hole sense a pressure that is greater than the free-stream static pressure. This latter pressure may be higher due to a lower local acceleration and pressure recovery in the separated flow. Thus, the pressure differences sensed by the holes in the yaw plane exceed the difference measured by the holes in the pitch plane. The resulting pressure coefficients reflect these differences.

The other major difference between the response of the two types of probes is that the k_s response of the prism probe, is somewhat skewed with respect to that of the of the angle-tube probe. The central hole of the prism probe is located only two probe diameters from its tip. As a result, the prism probe is probably subject to complex end-flow effects whereas the angle-tube probe had an extend support to improve flow symmetry.

Other repeatable non-symmetries appearing in the data apparently resulted from the inability to fabricate a symmetric probe. Differences between the calibration characteristics of different probes of similar size and geometry were also observed. These observations emphasize the need to individually calibrate each probe.

All calibration data were repeatable within 2% of the reference dynamic pressure when subjected to recalibration. These data consistently described the response of a particular probe; thus, they permit the successful application of the five-hole probes in a non-nulling mode.

Application of the calibration

When used in the non-nulling mode of operation, the five-hole probe provides five pressure measurements via a differential pressure transducer. These pressures are usually recorded relative to some reference pressure, p_{ref}

$$\Delta p_i = p_i - p_{ref}$$

Equ. 6

where the subscript i refers to the subject pressure. Local total and static pressure, pitch angle, yaw angle, and the three orthogonal velocity components can be computed from the probe data and the measured reference pressure. The interpolation procedures to perform these calculations have been computer-adapted and rely on the use of spline curves for all data specifications.

The values of $\Delta\beta$ and $\Delta\gamma$ are calculated from the grid of k_γ vs k_β. The values to be determined from the calibration data are a function of two independent variables, and thus a double interpolation procedure is required. Using the measured data, k_γ vs k_β can be calculate from Equ. 1 and 2. These experimental coefficients are represented by the "primed" superscripts, i.e., k_γ' vs k_β'. Individual spline curves are passed through the k_γ vs k_β calibration data for each value of $\Delta\beta$. At k_γ', the corresponding values of k_β are interpolated from the spline curves yielding the experimental local flow angle in the yaw plane, $\Delta\beta$. By interchanging the dependent and independent variables and forming the functional relationship between $\Delta\gamma$ and k_γ for a constant value of k_β , the experimental value of the local pitch angle, $\Delta\gamma$, can be determined.

From $\Delta\gamma'$ and $\Delta\beta'$, the experimental value of the static pressure coefficient, k_s', is obtained from the second part of the calibration data. Individual spline curves are passed through the k_s vs $\Delta\gamma$ data for each value of $\Delta\beta$. At $\Delta\gamma$ the corresponding values of k_s are interpolated from the spline curves, yielding the variation of k_s vs $\Delta\beta$. When the resulting curve is evaluated at $\Delta\beta$, the experimental value of the static pressure coefficient, k_s' results. The experimental value of the total pressure coefficient k_t', is evaluated in the same manner using the third graph of the calibration data.

When the absolute value of the reference pressure is recorded, the total and static pressure at the probe tip can be computed from k_t and k_s, respectively.

$$k_t^{/} = \frac{(\Delta p_1 - \Delta p_t)}{(\Delta p_1 - \overline{\Delta p})}$$

Equ. 7

and :

$$\Delta p_t = p_t - p_{ref}$$

Equ. 8

thus,

$$p_t = p_{ref} + \Delta p_1 - k_t^{/}(\Delta p_1 - \overline{\Delta p})$$

Equ. 9

In Eq. 9, all terms on the right of the equal sign are measured values except k_t', which was determined from the calibration data. In a parallel manner, the static pressure is computed from

$$p = p_{ref} + \overline{\Delta p} - k_s^{/}(\Delta p_1 - \overline{\Delta p}) \quad .$$

Equ. 10

By using Bernoulli´s equation, the magnitude of the local total velocity vector is:

$$w = \sqrt{\frac{2}{\rho}(p_t - p)} \; .$$

Equ. 11

By proper manipulation of the above equations, w could also be calculated directly from k_t' and k_s'.

$$w = (2/\rho)(\Delta p_1 - \Delta \overline{p})(1 + k_s^{/} - k_t^{/})$$

Equ. 12

When Reynolds number or wall proximity effects are present, they are included as correction to the calculated static pressure coefficients.

The manner by which the velocity is resolved is dependent upon the order of rotation employed during the calibration, i.e. upon the type of probe holder employed.

Systematic errors

Sources of error in the conventional probe measurement of the relative flow in turbomachinery blade passages are: (1) Reynolds number effects, (2) Mach number effects, (3) turbulence effects, (4) effects of pressure and velocity gradients, (5) wall vinicity effects, (a) probe near the annulus wall, (b) robe near the blades, (c) probe near the blade trailing edge, and (6) effects of probe blockage and probe stem.

A brief description of these sources of errors and an estimate of their magnitude are given below.

Reynolds number

Treaster and Yocum [10] give the following information on the influence of the Reynolds number.

Meaningful calibration data should be independent of the measured quantities. In most five-hole probe applications, velocity is the primary parameter to be measured; thus effect of changes in Reynolds number Re on the calibration data should be evaluated. To investigate these effect, the prism probes were calibrated in the open jet facility over an Re range of 2000 to 7000. The angle-tube probes were calibrated in the water tunnel at Re= 20000 and in the open-jet facility at Re= 8400.

For both types of five-hole probes, the total pressure, pitch and yaw coefficients were essentially unaffected by the Reynolds number variation. However, a measurable change in the static pressure coefficient was observed for both probe geometries. As an example, the effect of an Re variation from 3000 to 7000 at $\Delta\gamma$=30°, $\Delta\beta$=20° is shown to produce a maximum error in measured static pressure of 5,5% of the dynamic head and a 2.8% error in the velocity measurement.

To account for the dependency of the static pressure coefficient on the Reynolds number, a three parameter calibration in terms of $\Delta\gamma$, $\Delta\beta$, and Re would be necessary. In application, a corresponding iterative procedure in terms of the unknown Re would be required. These complications limit the practicality of the probes if they are to be used in studies characterized by large Re variations. However, several approaches are possible number: one is to calibrate at the expected Reynolds number, and another is to determine correction factors from the calibration data and to apply these as average values over small Re ranges. This latter approach is justified due to the relatively weak dependence of k_s' on Re . Both of these approaches are currently being employed.

Calibration of the probes used in the article of Dominy und Hodson [3] does not show appreciable variation with Reynolds number in the calibration characteristics at high Reynolds number. However, the effects of low Reynolds numbers (based on probe head diameter) may be appreciable. For the probes used,

calibrations were carried out approximately at a Reynolds number equal to that in the measured flow; hence, the Reynolds number effects are accounted for in the calibration.

A number or different, commonly used five-hole probe designs have been calibrated over a range of Reynolds numbers that are typical of those encountered in turbomachinery, and the existence of two separate Reynolds number effects has been confirmed by Sitaram [6]. The first result from separation of the flow from the probe head when the probe is at incidence. The effect of this upon the accuracy of yaw measurements is limited to Reynolds number below 15×10^3 for a 90° cone probe, 20×10^3 for a 60° cone probe, and 35×10^3 for a 45° cone probe. The geometry of the pressure-sensing holes has little effect on these limits. However, the hole geometry does affect the magnitude of the Reynolds number sensitivity, and it has been shown that probes with their pressure holes set perpendicular to the probe surface were less sensitive to changes in Reynolds number.

The second Reynolds number effect is apparent when the probe is at small or zero yaw angles and the effect was found to occur over a large part of the investigated range of Reynolds numbers. This effect is therefore significant even when probes are used in their nulled mode. The dependence of the dynamic pressure coefficient upon Reynolds number under these conditions is such that probes with pressure holes perpendicular to the surface should be employed whenever possible in preference to forward-facing designs.

The 90° pyramid cone displays similar characteristics to the corresponding cone type but the magnitude of the error arising from Reynolds number effects is reduced at high yaw angles. When nulled, no difference is observed between the performances of equivalent cone and pyramid probe.

A comparison of three conical, perpendicular probes shows that the probe with the largest cone angle was least sensitive to changes in Reynolds number. For this 90° probe the variation in yaw coefficient was equivalent to a maximum error of 0,7° while the error in the measurement of dynamic pressure was limited to approximately

3%. However the accuracy of dynamic pressure measurement is compromised over a greater range of Reynolds number.

An investigation of the effects of compressibility and free stream turbulence upon the sensitivity to Reynolds number shows that the basic flow patterns are unaffected by compressibility, whereas changes in free-stream turbulence may have a significant effect due to the influence of low Reynolds number separation bubbles (Dominy und Hodson [3])

Mach number

Dominy und Hodson [3] give the following information on the influence of the Mach number

In the above discussion the effects of the compressibility are considered to have little bearing on the sensitivity of these probes to Reynolds number changes and all the results have been obtained at a Mach number of 0,9. This assumption is based upon a series of calibration of the 45°, perpendicular cone probe at different Mach numbers. The difference between the yaw coefficient contours is only apparent at Reynolds numbers below 17×10^3. Thus, the yaw coefficient is insensitive to Mach number except at the lowest Reynolds number, a result that was later confirmed by the calibration of all of the cone probes over a range of Mach numbers up to Ma=1,2. In contrast and as might be excepted, the dynamic pressure coefficient is not independent of Mach number.

In the calibration and interpolation of the probe characteristics in the article for Dominy und Hodson [3] the flow is assumed to be incompressible, and the incompressible Bernoulli equation is used. The error caused by neglecting the effects of compressibility for the product probe amounts to about 1 percent at Ma=0,28, and the same magnitude of error may be assumed for the five-hole, disk, and sphere probes. Theses probes can be used in highly subsonic flow (up to Ma=0,7), if the first two terms of the binomial expansion of the isentropic Bernoulli equation is used in the calibration and interpolation of these probe characteristic. All the measurements

reported in this paper were carried out at Ma<0,3; Hence, this error estimate is irrelevant

Turbulence intensity

Sitaram [6] give the following information on the influence of the turbulence intensity

The conventional probes are usually calibrated in a well-controlled calibration tunnel where the flow turbulence is very low. They are used to measure relative flow in turbomachinery, where the turbulence fluctuations are large and cause error in pressure probes. Goldstein has theoretically investigated the direct effect of the turbulent velocity components on the measured probes measurement. This analysis is modified here to estimate the error due to turbulence for various probes employed in this investigation.

Five-Hole Probe. The pressure sensed by each hole can be written as:

$$p_i = p + k_i\left(\frac{1}{2}\rho w^2\right) + \alpha_i\left(\frac{1}{2}\rho\overline{q^2}\right)$$

Equ. 13

Where p_i refers to the i-th hole (i=1,2,3,4,5), k_i and α_i are constants for a particular hole, with their values less than unity. For example, for the center hole $k_i \approx 1$, $\alpha_i < 1$ for moderate pitch and yaw angles . The term $1/2\rho\overline{q^2}$ is the kinetic energy in turbulent fluctuation. The value of $p_1 - \overline{p}$ can be expressed as:

$$p_1 - \overline{p} = \overline{p_1 - \overline{p}} + \frac{1}{2}\rho\overline{q^2}\left[\alpha_1 - 0{,}25\left(\alpha_2 + \alpha_3 + \alpha_4 + \alpha_5\right)\right] =$$

$$\overline{p_1 - \overline{p}} + \frac{1}{2}\rho\overline{q^2}A$$

Equ. 14

$$A = \alpha_1 - 0{,}25\left(\alpha_2 + \alpha_3 + \alpha_4 + \alpha_5\right)$$

Equ. 15

Similarly, neglecting terms of small order (e.g., $\overline{q^2 q^2}$).

$$k_\gamma = \frac{p_4 - p_5}{p_1 - \overline{p}} = \overline{k_i}\left(1 - \frac{1/2\rho\overline{q^2}A}{\overline{p_1 - \overline{p}}}\right)$$

Equ. 16

Where $\overline{p_1 - \overline{p}}, \overline{k_i}$ refer to values in the absence of turbulence (i.e. during calibration). Using similar procedure expressions for k_β, k_t can be derived. An estimate of the errors due the turbulence is carried out below assuming that the central hole senses mostly total pressure and the others, mostly the static pressure. Reasonable assumptions for α_1 is 1.0 and α_2, α_3, α_4, α_5 are 0.33 since the central hole senses, approximately, the total turbulent kinetic energy, while the static hole sense the normal component. Hence, A=0,33, and assuming $p_1 - \overline{p} \approx 1/2\rho w^2$, the error in k_γ is 0,67% for 10% turbulence intensity and 2,68% for 20% turbulence intensity. There will be corresponding errors in angles and pressures. Thus for a 10% turbulence intensity the estimate value of the error in total velocity is approximately 0,33%, while the errors in velocity components vary depending on the pitch and yaw angles.

Spherical Head Static-Stagnation Pressure Probe. The static pressure measured by the spherical static-pitot pressure probe is not affected by the turbulence in the flow, since the trips around the sphere generate turbulence when the probe is calibrated in a uniform flow. Goldstein´s analysis for the pitot probe error in the turbulent flow shows the percentage error in the stagnation pressure of about 0,5 times turbulence intensity. The same magnitude may be assumed for the error in the stagnation pressure measured by the central hole of the sphere probe. Hence, the sphere probe measures slightly higher stagnation pressures and velocities in a turbulent flow.

It has been demonstrated in the article of Dominy und Hodson [3] that at least part of the influence of Reynolds number upon probe calibrations is due to the

changing nature of the separation that exist at all flow angles; changes that stem from the influence that Reynolds number exerts upon the transition processes within the separation bubbles. Since free-stream turbulence is also known to influence transition processes, a brief study of the influence of free-stream turbulence was undertaken at low speed using a large-scale model of the 60°, forward-facing probe. This model was calibrated in a low turbulence stream and then again behind a biplanar turbulence grid with a mesh spacing equal to 85% of the probe diameter. The grid size was chosen so as to create turbulence of a similar relative scale to that occurring in practical environments and a free stream turbulence intensity (streamwise component) of 40% was generated compared with < 0,1% without no grid fitted.

It is evident that the intensity of the turbulence does affect the probe calibration when $Re<20\times10^3$ when, in the case of low turbulence, a separation bubble is known to exist . Thus free-stream turbulence may influence the accuracy of probes that are sensitivity to Reynolds number (Dominy und Hodson [3])

Velocity Gradient

Sitaram [6] give the following information on the influence of the velocity gradient:

Principal Effects

The probes used in the investigation are calibrated in a uniform flow, but they are used to measure relative flow in turbomachinery rotors where step gradients in pressure and velocity exist (e.g. rotor wakes, boundary layer and tip leakage flow). These gradients affects the probe performance in the followings ways:

1- The probe indicates the reading at a location different from the geometry center of the probe. This effect, known as the displacement effect, has been investigated extensively for the pitot tube and a the three-hole probe.

2- In multi-hole probes, each hole is located in a differing pressure field; hence, an additional error is introduced. This will be called spatial error for a five hole probe.

3-The presence of the probe in a velocity gradient causes deflection of the streamlines toward the region of lower velocity. This deflection causes the probe to indicate pressures in excess of that existing at the same location in the absence of the probe.

An estimate of the spatial error due to gradients in the flow for a five hole probe is given below.

Assuming the pressure gradient in the flow is known (dp_t/dy), the following relationships my be written for the five hole-probe used in the investigation:

$$p_1 = k_1 p_t$$

Equ. 17

$$p_i = k_i \left(p_t - \frac{dp_t}{dy} 0{,}35d \right) \qquad \text{i= 2, 5}$$

Equ. 18

$$p_i = k_i \left(p_t + \frac{dp_t}{dy} 0{,}35d \right) \qquad \text{i= 3, 4}$$

Equ. 19

Where p_t is the total pressure and the value 0,35 results from the geometry of the probe head, which is a hemisphere and has four holes at 45° to the axis of the probe head in two mutually perpendicular planes. Hence, the calibration coefficient for the five hole probe is given by:

$$p_1 - \overline{p} = p_1 - 0{,}25(p_2 + p_3 + p_4 + p_5) =$$
$$= k_1 p_t - 0{,}25\left\{\left(k_2 + k_3 + k_4 + k_5\right)p_t + (k_3 + k_4 - k_2 - k_5)\frac{dp_t}{dy}0{,}35d\right\}$$
$$= (\overline{p_1 - \overline{p}})(1 + A)\,,$$

Equ. 20

where A depends on the pressure gradient, orientation and geometry of the probe. Hence to the first approximation:

$$\mathrm{k}_\beta \approx \overline{k_\beta}(1 - A)$$

Equ. 21

Similarly, other coefficients are modified.

The disk and sphere probes are not subjected to the above error, since the holes are either along the same axis as in the sphere probe or not subject to pressure gradients as in the disk probe. All three probes are subjected to the displacement effects, which may be assumed to be the same as that of a pitot tube.

$$\frac{\delta}{d} = 0{,}021\frac{d_h}{d}$$

Equ. 22

Where δ is the displacement of probe measuring point from the probe geometric center and d_h is the diameter of the probe hole.

Wall Vicinity Effects

Whenever a probe is located near a solid surface, the flow acceleration in that region introduces an additional error. In the measurement of flow in a turbomachinery, the probe is placed closed to many solid surface, such as annulus wall and blades. A discussion of these errors follow.

Experimental results of Sitaram [6] for a prism type five-hole probe indicate an increase in velocity measured by the probe close to a solid surface. The study of Lakshminarayana [6] shows the error in velocity measured by the five-hole probe, when the probe is adjacent to a blade. The error is negligible, when the distance between the probe and the blade is more than two probe diameters. Similar magnitude of error in velocity measured by the disk probe and the sphere probe may be anticipated.

When a probe is very near a blade trailing edge, it is subjected to the following effects: (1) viscid and inviscid interference between the probe and the trailing edge, (2) area blockage, and (3) velocity and pressure gradient discussed earlier.

The complexity of the interaction between the probe and the trailing edge prohibits an estimate of the error in the probe measurement, and the results very near the trailing edge are to be viewed with caution.

The experimental investigation of wall-proximity effects on the calibration characteristics of the prism probes was conducted in the presence of a sharp-edge flat plate that spanned the working area of the open jet facility (Treaster and Yocum [10]). With the flat plate mounted parallel to the flow and with the measuring station located 12,7 cm downstream of the leading edge, the local boundary-layer thickness was small compared to the probe diameter. Thus, any changes in the calibration characteristics in the proximity of the plate were attributed to a probe-plate potential flow interaction as opposed to boundary-layer effects. It should be noted that errors in boundary-layer measurement are primarily a function of the local velocity gradient and the size and spacing of the holes. This implies that the problem in the boundary-layer measurements is one of probe selection and not one of calibration.

Calibration were conducted at Re= 7000 for the probe both approaching and being withdraw through the plate. For both installations, $\Delta\beta$ was varied from –30 ° to +30° at each of the selected measuring points while maintaining $\Delta\gamma$=0° and a perpendicular probe-plate orientation.

These latter restrictions were necessary since, with the present apparatus, it was impossible to change the flow angle $\Delta\gamma$, without also altering the orientation of the probe with respect to the plate.

Although the effects caused by a wall may be a function of both $\Delta\gamma$ and $\Delta\beta$ as well as the distance to the wall, the pitch angle could not be varied with introducing the probe-plate orientation as an additional variable. Thus, to apply the wall effects data, the assumption must be made that the probe response is independent of pitch angle. This assumption appears reasonable from observation of the available data. The changes in the calibration data as a function of distance are quite similar for the various yaw angles tested. This suggests that the wall-proximity effects are primarily a function of distance only. Additional investigations in this area would require an apparatus capable of changing $\Delta\gamma$ while maintaining the same probe-plate orientation. At the present time, it seems unlikely that such an apparatus can be developed.

For the other configuration in which the probe was withdraw through the plate, all calibration coefficients were altered within two probe diameters of the plate. These effects are illustrated by k_s versus k_β. This observed variation in all coefficients makes these probes essentially impractical for measurement when the center hole is within two probe diameters of the wall. Thus a limitation of two-probe diameters is imposed as the probe is withdrawn through a wall, whereas the probe´s geometry imposes a physical limitation of the same magnitude as the probe approaches a wall.

Restricting the use of the probe distances greater than two probe diameters does not eliminate all wall interaction effects. k_s is still affected at greater distances. These effects of the wall, when limited to k_s only, can be incorporated in the data reduction program in a similar manner to that used for the Reynolds number effects program.

The probes have been used to survey the three-dimensional flow fields in the propeller planes of surface ships, as well as in the inlet and exit planes of other rotating blade rows. These results agreed well with data measured by other types of probes and instrumentation.

A factorally designed experiment aimed at quantifying the relative effects and interactions of five independent variable on the near wall performance of wedge type traverse probes has been completed Smout and Ivey [8]. The probe interface piece length and fillet geometry, the probe pitch angle and the flow Mach number and turbulence intensity have all been investigated. This has involved modifying and fully characteristic the flow in a 200 mm diameter, closed section wind tunnel to achieve a facility in which a probe´s ability to measure static pressures under a wide range of conditions may reliable tested.

The length of the interface piece is strongly influential. It is shown that moving the wedge head away from the influence of the circular stem by increasing this length leads both to a marked reduction in wall proximity effects, and a change in the free-stream static pressure coefficient. Near wall performance deteriorates when the probe is operated at negative pitch angles, which is consistent with the interface piece length conclusion. The third highly significant variable is the free stream Mach number, an increase in again reduces a probe ability to measure free stream static pressure close to the wall of introduction. Less important, but still of some statically significance, are the effects of a stem fillet and the free stream turbulence intensity.

It is suggested that stemwise flows driven by local pressure gradients along the probe length may be responsible for the wall proximity effects, and some of the features seen in the probe radial traverse curves support this idea. However, the mechanism by which the precise flow structure around the probe head and stem is modified by the presence of a wall can not be inferred from this investigation.

Effects of Probe Blockage and Probe Stem

Probes used for the flow measurement effectively block the flow area. For the probes used in the investigation Sitaram [6], the probe blockage is about 2 to 3% of blade spacing. Hence, the axial velocity increases by this amount, so the measured velocities are to be decreased by the same amount.

The probe stem supporting the probe causes interference with the flow near the tip. Experimental results for the pitot and static probes indicate that this effect is negligible when the distance between the probe tip and the axis of stem is more than four times the stem diameter from the stem axis. Hence, this error is negligible.

6 Method of Streamline Projection

A first estimation of the coefficients of calibration is given by the streamline projection method. This simple method can also be used for a first approximation of the influence of velocity gradients on the error of the three-hole probe. The streamline projection method is based on the assumption that the velocity component normal to the probe surface acts as a fraction of the dynamic pressure. Therefore, the holes of the probe sense a pressure equal to the static pressure plus the corresponding fraction of the dynamic pressure. Figure 3 shows a sketch of the probe head with a wedge angle δ. The angle between the velocity w and the axis of symmetry is $\Delta\beta$.

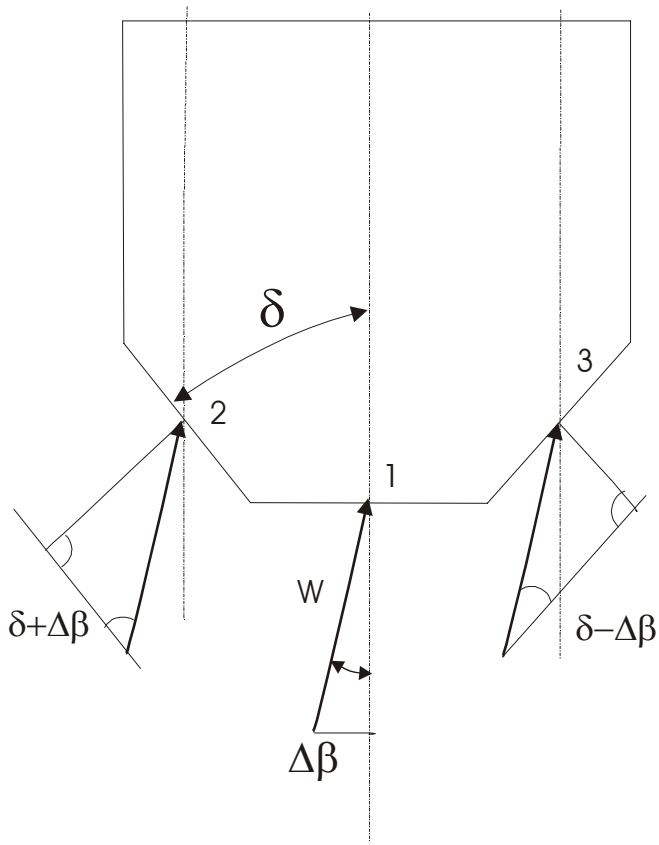

Fig. 3: Angles used for the streamline projection method

Under this assumption, the three holes sense the following pressures:

$$p_1 = p + \rho \frac{(w \cdot \cos \Delta\beta)^2}{2}$$

Eq. 23

$$p_2 = p + \rho \frac{(w \cdot \sin(\delta + \Delta\beta))^2}{2}$$

Eq. 24

$$p_3 = p + \rho \frac{(w \cdot \sin(\delta - \Delta\beta))^2}{2}$$

Eq. 25

In the next step, the individual hole pressures are made dimensionless. Generally, the is called hole coefficients are.

$$k_i = \frac{p_i - p}{\frac{1}{2}\rho w^2} \qquad \text{for i = 1,2,3}$$

Eq. 26

In Eq. 26 p stands for the static pressure, Under the streamline projection approximation, the hole coefficients are as follows:

$$k_1 = \cos^2 \Delta\beta$$

Eq. 27

$$k_2 = \sin^2(\delta + \Delta\beta)$$

Eq. 28

$$k_3 = \sin^2(\delta - \Delta\beta)$$

Eq. 29

The coefficient of the central hole 1 depends only on the flow angle $\Delta\beta$. The coefficients k_2 and k_3 of the holes 2 and 3 depend an the flow angle $\Delta\beta$ as well as on the wedge angle δ. For the probe under investigation δ=30° and the corresponding hole coefficients are plotted in Fig. 4.

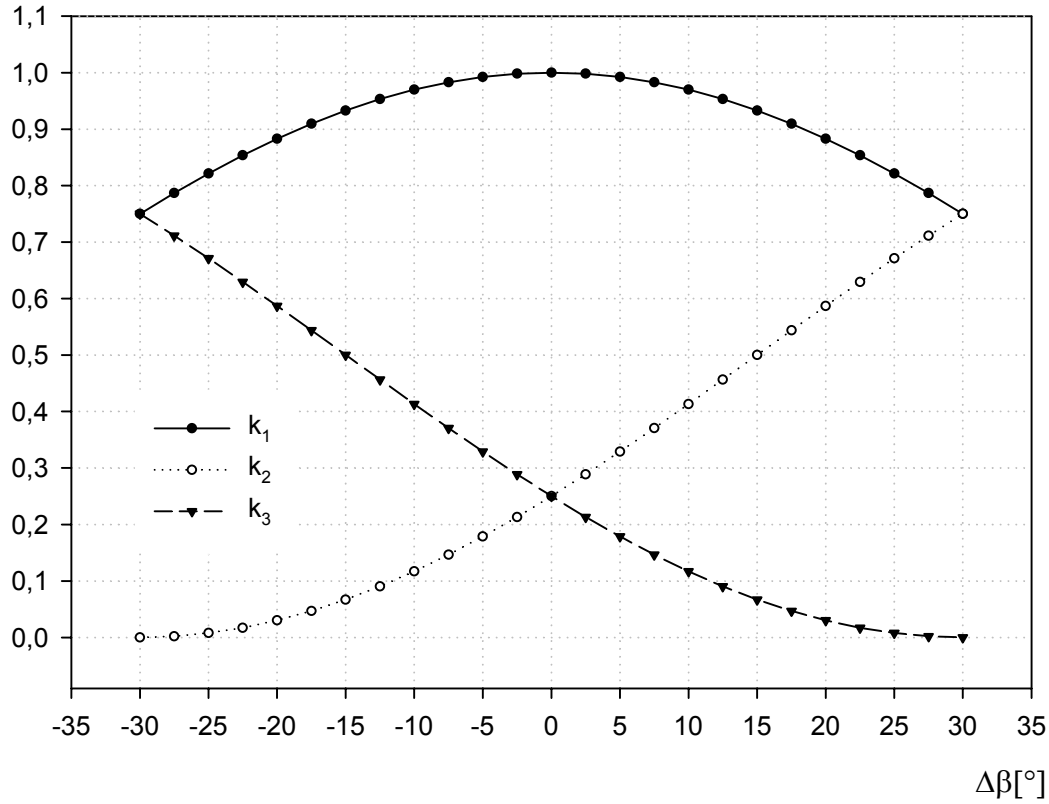

Fig. 4: Theoretical hole coefficients k_1, k_2 and k_3

For the practical application of the three-hole probe, the calibration coefficients are calculated from the hole coefficients. This calibration coefficients should give a

direct relation between the three hole pressures and the flow angle, the total pressure and the static pressure. In the literature, a variaty of different descriptions can be found. The present investigation uses the calibration coefficients defined by Treaster and Yocum [10].

Directional coefficient:

$$k_\beta = \frac{p_2 - p_3}{p_1 - \overline{p}} = \frac{k_2 - k_3}{k_1 - \overline{k}}$$

Eq. 30

Total pressure coefficient:

$$k_t = \frac{p_1 - p_t}{p_1 - \overline{p}} = \frac{k_1 - 1}{k_1 - \overline{k}}$$

Eq. 31

Static pressure coefficient:

$$k_s = \frac{\overline{p} - p}{p_1 - \overline{p}} = \frac{\overline{k}}{k_1 - \overline{k}}$$

Eq. 32

The mean pressure $\overline{p}$ and the mean hole coefficient $\overline{k}$ are obtained from

$$\overline{p} = \frac{p_2 + p_3}{2} \quad \text{and} \quad \overline{k} = \frac{k_2 + k_3}{2},$$

Eq. 33

respectively.

Using the concept of the streamline projection, the calibration coefficients can be related directly to the flow angle $\Delta\beta$ and the wedge angle δ.

Direction coefficient:

$$k_\beta = \frac{p_2 - p_3}{p_1 - \overline{p}} = \frac{\sin^2(\delta + \Delta\beta) - \sin^2(\delta - \Delta\beta)}{\cos^2 \Delta\beta - \frac{1}{2}\left(\sin^2(\delta + \Delta\beta) + \sin^2(\delta - \Delta\beta)\right)}$$

Eq. 34

Total pressure coefficient:

$$k_t = \frac{p_1 - p_t}{p_1 - \overline{p}} = \frac{-\sin^2 \Delta\beta}{\cos^2 \Delta\beta - \frac{1}{2}\left(\sin^2(\delta + \Delta\beta) + \sin^2(\delta - \Delta\beta)\right)}$$

Eq. 35

Static pressure coefficient:

$$k_s = \frac{\overline{p} - p}{p_1 - \overline{p}} = \frac{\sin^2(\delta + \Delta\beta) + \sin^2(\delta - \Delta\beta)}{2\left[\cos^2 \Delta\beta - \frac{1}{2}\left(\sin^2(\delta + \Delta\beta) + \sin^2(\delta - \Delta\beta)\right)\right]}$$

Eq. 36

The theoretical calibration coefficients for the three-hole probe under investigation (δ=30) are plotted in Fig. 5.

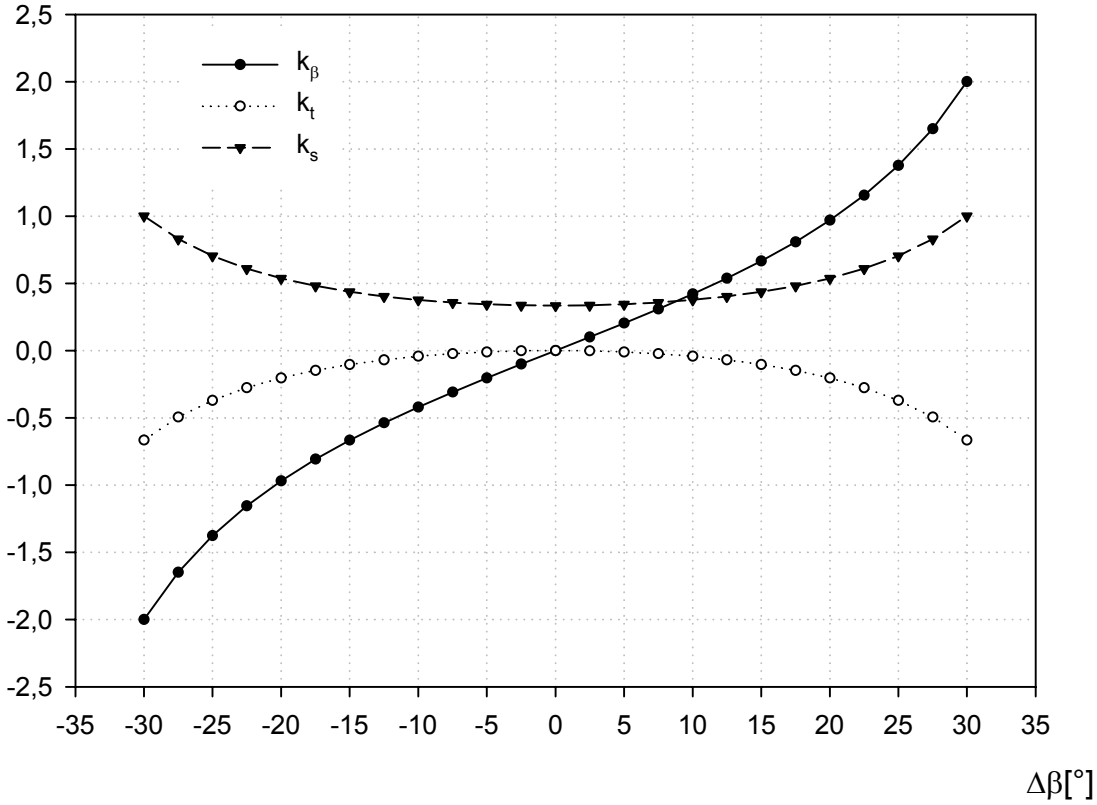

Fig. 5: Theoretical calibration coefficients k_β, k_t and k_s

As can be seen from Fig. 5, there is a definite relation between the flow angle $\Delta\beta$ and the directional coefficient k_β. For small flow angles, the relationship is nearly linear and it follows from a Taylor series expansion:

$$k_\beta = \frac{\pi}{45°} \tan\delta \cdot \Delta\beta$$

Eq. 37

The slope of the curve of the direction coefficient is a measure for the sensitivity of the probe on the flow direction. As can be seen from Eq. 37 the sensitivity increases with increasing wedge angle δ.

The streamline projection method can be used for a first approximation of the influence of a velocity gradient on the direction measurement of a three-hole probe.

Fig. 6 shows the velocity distribution upstream of the probe head. The direction of the flow corresponds to the line of symmetry. This is often nearly the case for flow measurement downstream of turbine of compressor cascades. Since the flow direction can be estimated by the sin-rule the probe head can be aligned in the flow direction.

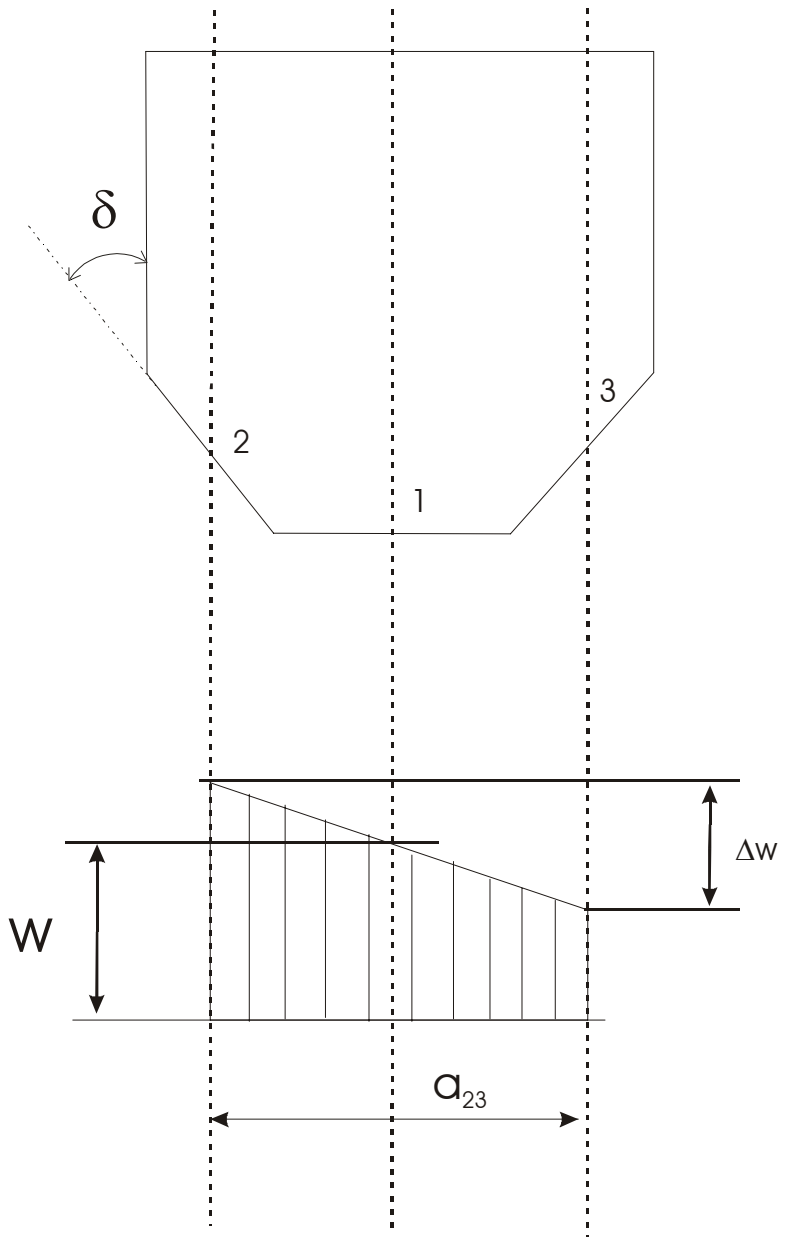

Fig. 6: Model of gradient effect with three probe hole

The velocity gradient is characterized by $\Delta w / a_{23}$ whereas the velocity magnitude upstream of the centre hole is w. In contrast to the case of constant velocity, the side holes 2 and 3 now sense different pressures due to the velocity gradient. The static pressure p is assumed as constant and the concept of the streamline projection gives for the three hole pressures:

$$p_1 = p + \rho \frac{w^2}{2}$$

Eq. 38

$$p_2 = p + \rho \left(w + \frac{\Delta w}{2} \right)^2 \frac{\sin^2 \delta}{2}$$

Eq. 39

$$p_3 = p + \rho \left(w - \frac{\Delta w}{2} \right)^2 \frac{\sin^2 \delta}{2}$$

Eq. 40

The velocity gradient induces a pressure difference between hole 2 and 3.

$$p_2 - p_3 = \delta \cdot w \cdot \Delta w \cdot \sin^2 \delta$$

Eq. 41

For the calculation of the directional coefficient, the denominator $p_1 - \overline{p}$ is derived using Fig. 6:

$$p_1 - \overline{p} = \rho \frac{w^2}{2} \left(1 - \sin^2 \delta \left(1 + \frac{1}{4} \left(\frac{\Delta w}{w} \right)^2 \right) \right)$$

Eq. 42

As will be seen later, the velocity deficit Δw downstream of a blade row is small compared with the velocity magnitude w. Therefore,

$$1+\frac{1}{4}\left(\frac{\Delta w}{w}\right)^2 \approx 1$$

Eq. 43

and

$$p_1-\overline{p} \approx \rho\frac{w^2}{2}\left(1-\sin^2\delta\right).$$

Eq. 44

The directional coefficient

$$k_\beta=\frac{p_2-p_3}{p_1-\overline{p}}=2\left(\frac{\Delta w}{w}\right)\tan^2\delta$$

Eq. 45

can be related to the linear approximation

$$k_\beta=\frac{\pi}{45°}\tan\delta\cdot\Delta\varepsilon$$

Eq. 46

This step requires that the measurement error of the flow angle $\Delta\varepsilon$ is small. As result it follows

$$\Delta\varepsilon=\frac{\pi}{45°}\tan\delta\cdot 2\left(\frac{\Delta w}{w}\right).$$

Eq. 47

Since the static pressure is assumed as constant, the velocity gradient corresponds to a total pressure gradient. In the literature the total pressure gradient is made dimensionless with the hole distance a_{23} as well as the dynamic pressure upstream of the center hole:

$$K = \frac{dp_t}{dy} \cdot \frac{2a_{23}}{\rho w^2} = \frac{dw}{dy} \cdot \frac{2a_{23}}{w} = 2\left(\frac{\Delta w}{w}\right)$$

Eq. 48

As a general result, the streamline projection method gives the following equation for the measurement error of the flow angle:

$$\Delta\varepsilon = \frac{\pi}{45°} \tan\delta \cdot K$$

Eq. 49

As can be seen from Eq 49, the measurement error is direct proportion to the wedge angle δ of the probe head and to the nodimensional velocity gradient K. For the three-hole probe under investigation (δ=30°)

$$\Delta\varepsilon = 8{,}3 \cdot K = C \cdot K \,.$$

Eq. 50

As can be seem from Eq (50), the error of the flow angle $\Delta\varepsilon$ is proportional to the non dimensional velocity gradient K. Eq.(50) is plotted in Fig. 7 with the constant C= 8,3 obtained from the method of streamline projection. Additionally, a curve with C= 13,2 is plotted in Fig. 7. This value had been obtained by Ikui and Inou [5] by an experimental calibration of a cobra probe (δ=45°). The investigation of the gradient effect reduces to the experimental determination of the constant C by a calibration procedure.

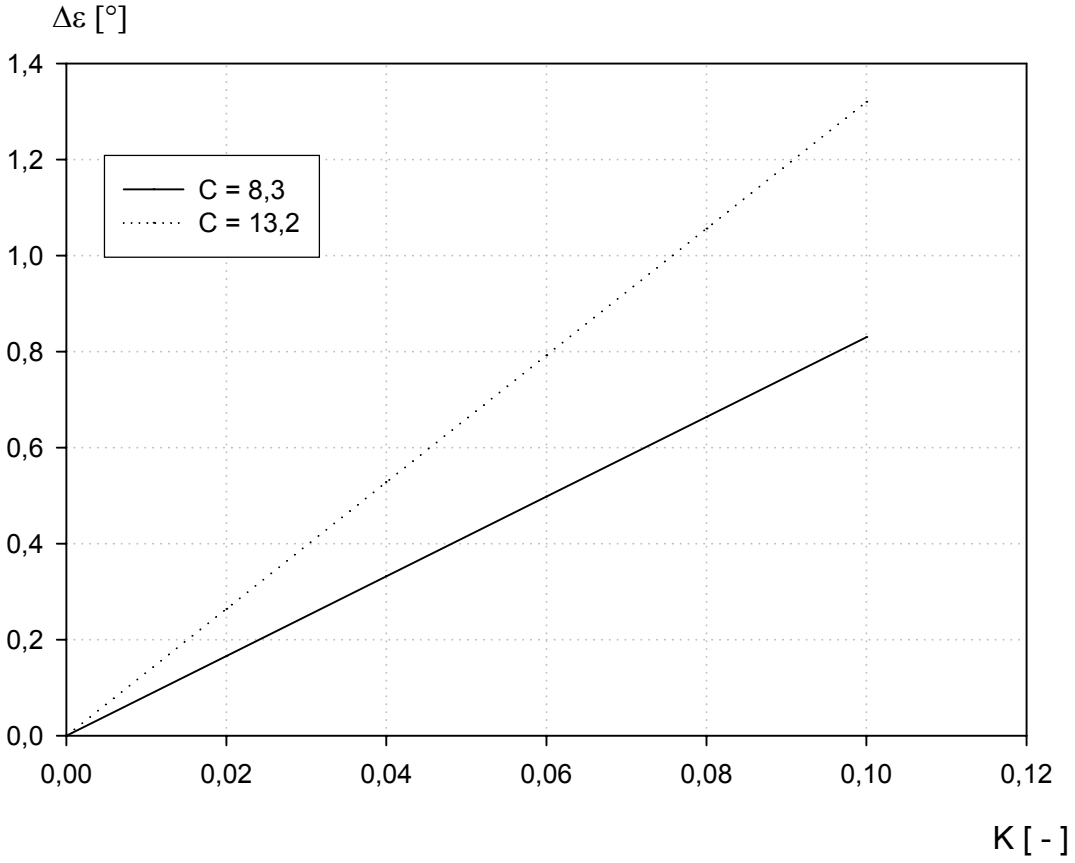

Fig. 7: Flow angle error Δε as a function of the nondimensional velocity gradient K

7 Experimental Setup

The experimental investigations are performed in two different wind tunnels:

- Free jet wind tunnel
- Modified cascade wind tunnel

The principal setup of the free jet wind tunnel is shown in Fig. 8. This wind tunnel is used for the calibration of the three-hole probe under different angles $\Delta\beta$ but constant speed w(y). The wind tunnel consists of a nozzle with 120 mm diameter. Since the diameter of the setting chamber is 1000 mm, the contraction ratio of the nozzle is about 1:69,4. The air is supplied by a radial blower with variable speed. Three different velocities are investigated. This results in Reynolds numbers of 3.500, 7.400, and 11.100, respectively. The three-hole probe is placed 190 mm downstream of the nozzle exit plane. It can be turned to adjust different flow angles $\Delta\beta$. Flow angles ranging from $\Delta\beta$ = -30 ° to $\Delta\beta$= +30 ° are performed in steps of 2,5°.

Fig. 8 shows also the measurement equipment of the free jet wind tunnel. A HP3852A data acquisition and control unit is equipped with a HP44711A 24 channel high-speed multiplexer, a HP 44702B 13 bit high-sped voltmeter and a HP44724A 16 channel digital output. The multiplexer and the voltmeter are used for the measurement of the piezoresistive pressure transducers (HONEYWELL) and the Pt 100 resistor thermometer. The digital output controls the pressure scanning box (FURNESS CONTROLS). The HP3852A and the personal computer are connected via the GPIB bus. The entire system is controlled by the software LabVIEW5. The turbulence intensity of the core of the free jet is about 1 %. It is measured with a single hot-wire probe DANTEC 55P11.

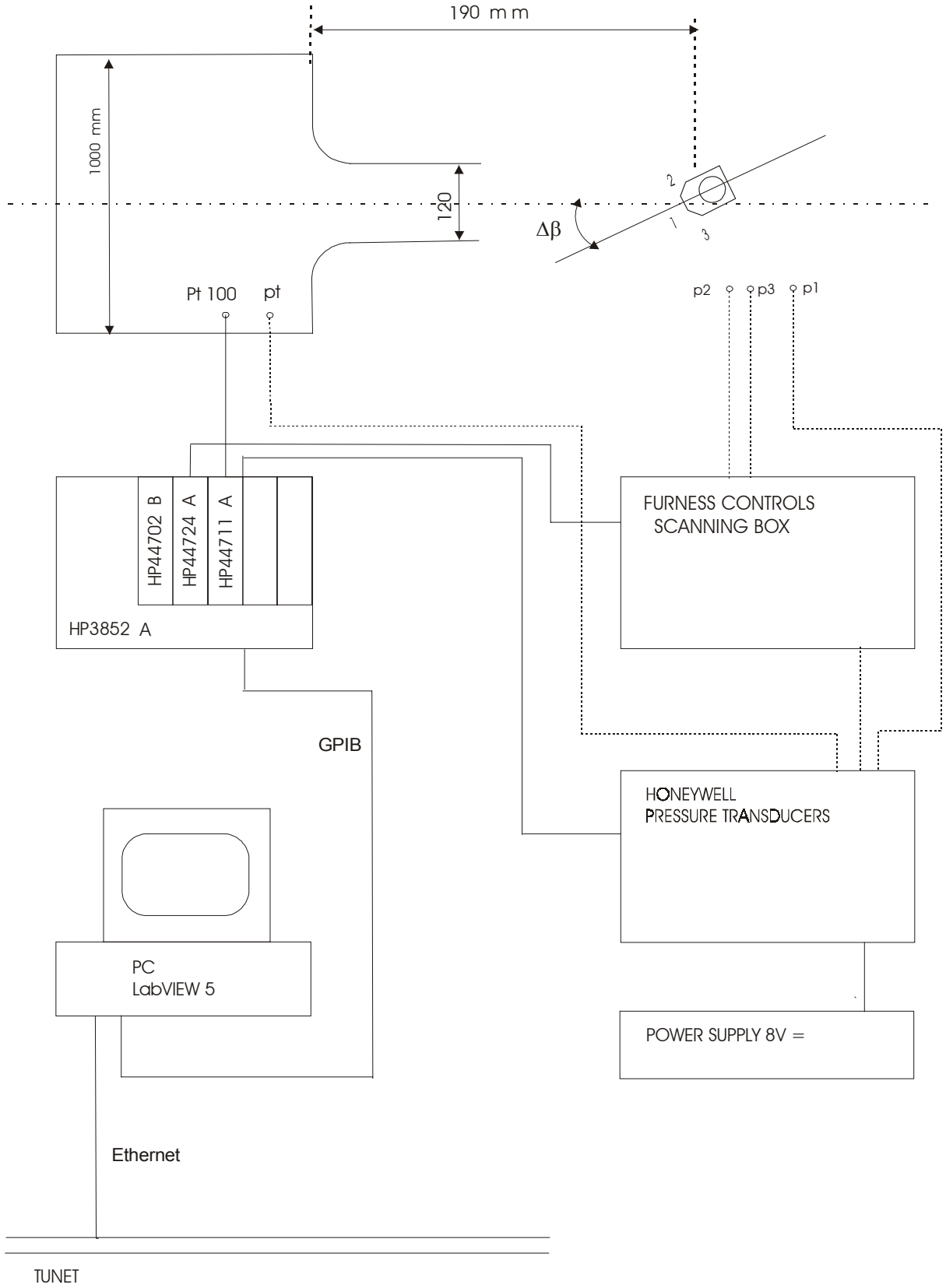

Fig. 8: Free jet wind tunnel

The cascade wind tunnel is modified to produce a turbulent boundary layer for the investigation of the gradient effect. Figure 9 shows the modified cascade wind tunnel as well as the measurement equipment. The working section of the wind tunnel is a rectangle 150 mm to 400 mm. Air is supply by an axial blower with constant rotational speed but variable inlet guide vanes. The measurement plane is 29 mm upstream of the exit of the wind tunnel duct. A natural turbulent boundary layer develops at the duct walls. The three-hole probe is traversed, through this boundary layer perpendicular to the bottom duct wall (y-direction). The traversing is performed by a DANTEC traverse controlled by a ISEL C10C-E/A stepping motor control. The pressure measurement is identical to the equipment of the free jet wind tunnel (Fig. 8).

Prior to the investigation on the three-hole probe, the velocity distribution in the boundary layer is measured with a hot-wire probe. The entire hot-wire measurement setup is shown in Fig. 10. It consists of a DANTEC 90N10 frame with three modules 90C10. One module is used with a boundary layer probe 55P15. The probe is traversed in the measuring plane with the DANTEC traverse. During the hot-wire measurement, the temperature is measured with a thermocouple to compensate the temperature drift of the air flow. Prior to the measurement the velocity calibration of the hot-wire probe is performed in the DANTEC 90H02 flow unit. This miniature free jet wind tunnel is connected via an air filter to the air supply of the laboratory (7 bar). King´s law is used for the approximation of the relationship between velocity and bridge voltage. The conversion of the analog signal to digital form is performed by a scanning box SCB-68 (NATIONAL INSTRUMENTS) and a AT-MI0 16E-10 card. StreamWare3 is used as control software for the hot-wire anemometry system.

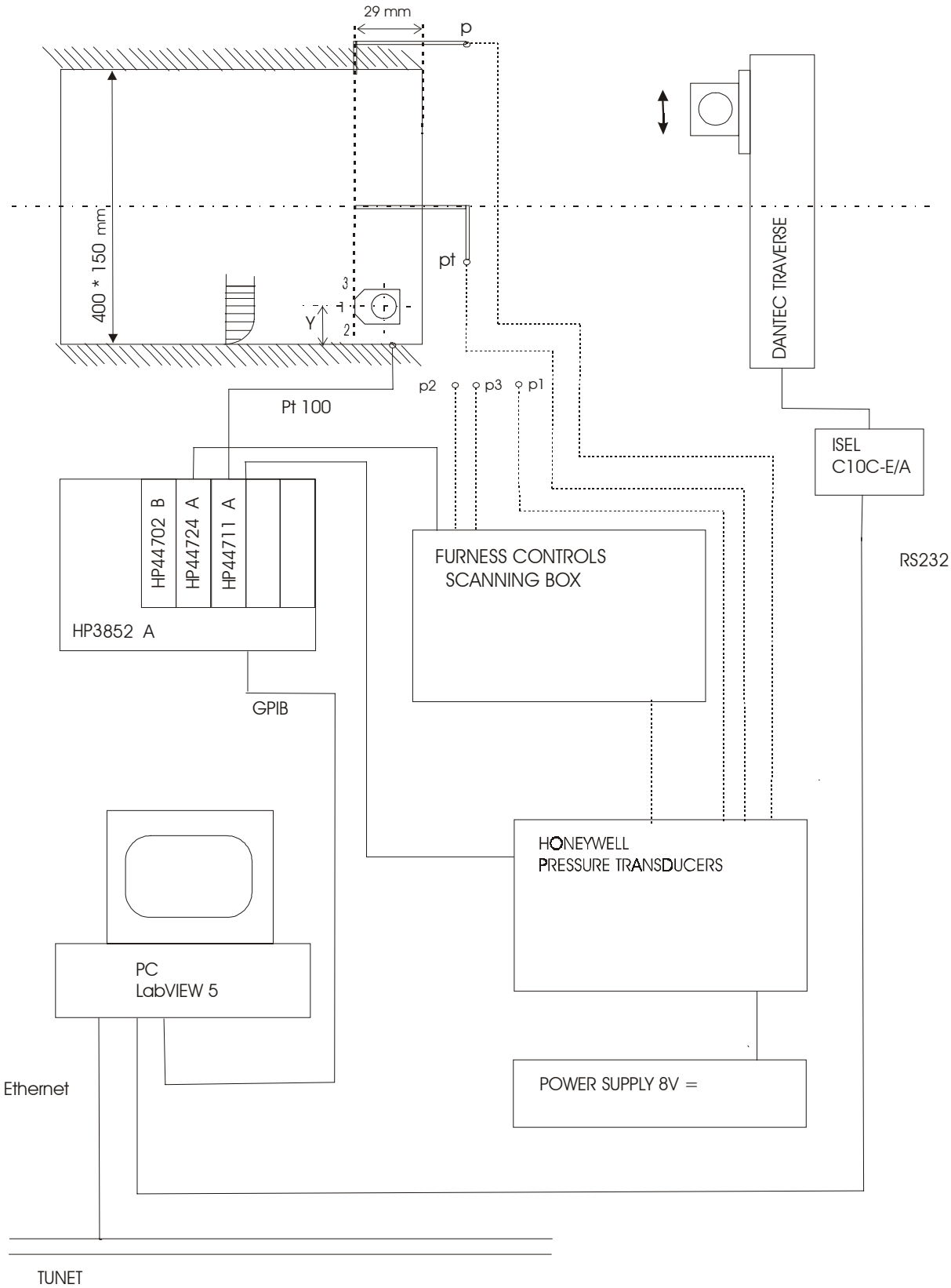

Fig. 9: Modified cascade wind tunnel

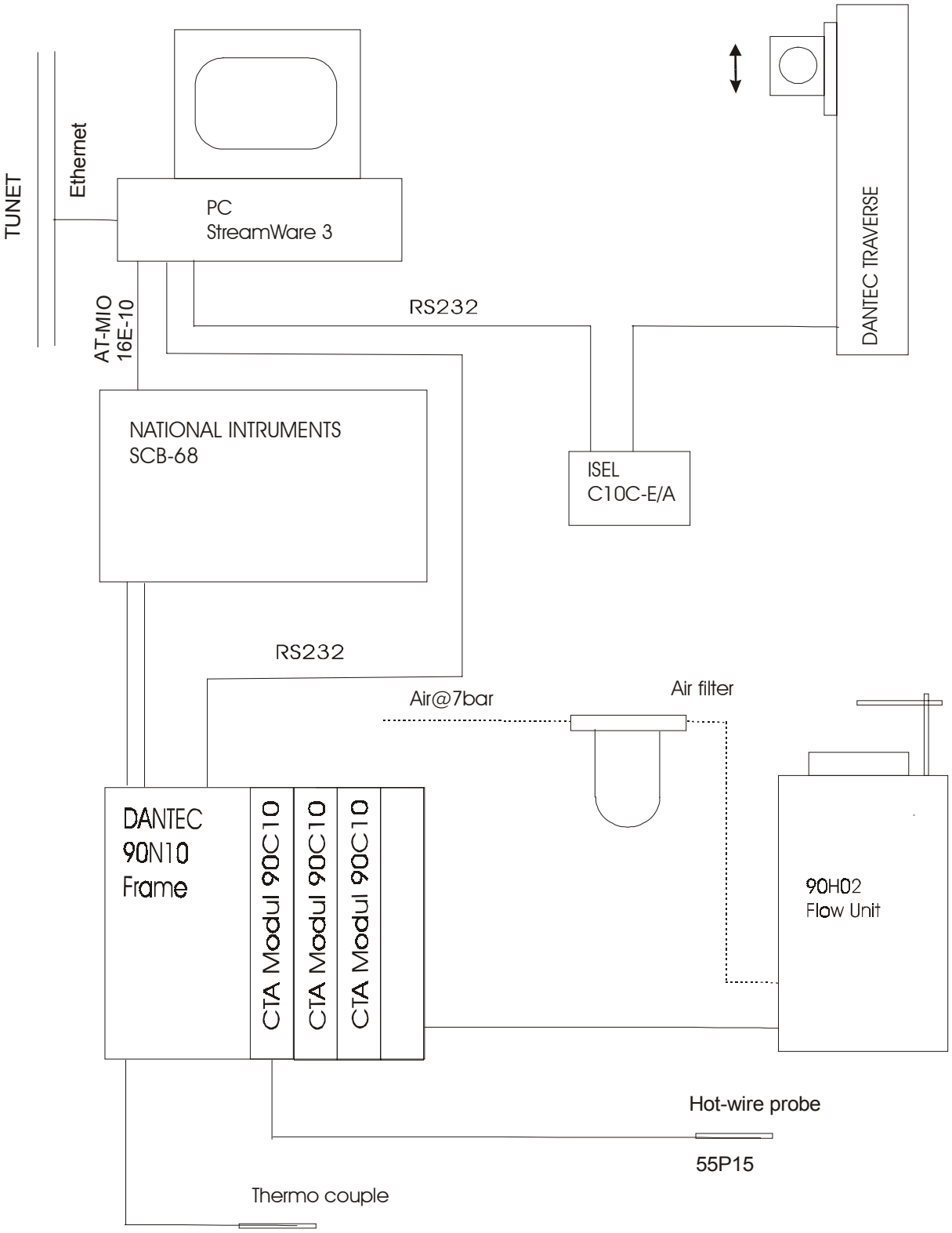

Fig. 10: Hot-wire anemometry system

8 Experimental Procedure

In a first step, the calibration curves in a velocity field without gradients are obtained from the free jet wind tunnel. The nozzle exit velocity, and therefore, the probe Reynolds number is controlled by the rotational speed of the radial blower. Three different Reynolds numbers (Re=3500, 7400 and 11100) are investigated, whereas Re= 7400 is the typical Reynolds number for the consecutive investigation of the gradient effect. At a fixed angular setting $\Delta\beta$ of the three-hole probe, the three hole pressures p_1, p_2, p_3 are measured. Furthermore, the total pressure p_t and the temperature t in the plenum of the free-jet wind tunnel are measured. The static pressure in the free jet corresponds to the ambient pressure, which is measured with a barometer. All pressures, except the ambient pressure, are measured as relative pressures to the ambient pressure.

After the calibration in the free jet wind tunnel, the influence of the velocity gradient on the behaviour of the three-hole probe is investigated in the modified cascade wind tunnel. For reference purposes the velocity distribution in the boundary layer at the botton wall is measured with the 55P15 boundary layer hot-wire probe. The minimum distance from the wall is 1mm and a total of 200 points of Δy =0,5mm are taken. At each point N=51200 samples at a sampling rate SR= 50 kHz are taken. This results in a sampling time T= N/SR =1024 ms per point. The velocity distribution, obtained from the hot wire measurement is used for the derivation of the nondimensional velocity gradient.

$$K = \frac{2a_{23}}{w} \cdot \left(\frac{\Delta w}{\Delta y} \right)$$

Eq. 51

The distribution of the turbulence intensity

$$Tu = \frac{\sqrt{\overline{w`^2}}}{w}$$

Eq. 52

in the boundary layer is a further result of the hot-wire measurement After the hot-wire measurement the three-hole probe is inserted into the wind tunnel through a slot at the side wall. The head of the probe is position in the midsection and aligned parallel to the bottom wall. It can be expected that the flow direction in the boundary layer is parallel to the wall and therefore the flow angle measured by the three-hole probe should be zero. Each deviation from the zero flow angle can be interpreted as an error induced by the velocity gradient. The minimum distance between the probe head and the end wall is dictated by the diameter of the probe stem. Since this diameter is 6 mm, a minimum distance of 3 mm results. A total of 100 points at intervals Δy=0,5 mm are investigated. At each point the three hole pressure p_1, p_2 and p_3 , the total pressure (pitot probe), the static pressures and the temperature are measured.

9 Results of Calibration with Constant Velocity

The calibration coefficients k_β, k_t and k_s for the three Reynolds numbers (Re = 3500, 7400 and 11150) are presented in Fig. 11 to Fig. 13. The calibration coefficients are plotted versus the relative flow angle $\Delta\beta$ and can be compared with the values obtained from the streamline projection method (Fig 5). Each value of the direction coefficient k_β corresponds to an individual flow angle $\Delta\beta$. The relationship is nearly linear for $-15° < \Delta\beta < 15°$. However, the measured distribution of k_β gives a higher sensitivity on the flow angle $\Delta\beta$. The maximum total pressure coefficient k_t occurs at $\Delta\beta \approx 2°$, due to the manufacturing inaccuracy of the front plane of the probe head. The static pressure coefficient k_s is nearly independent of the flow angle $\Delta\beta$ and some influence of the Reynolds number can be observed.

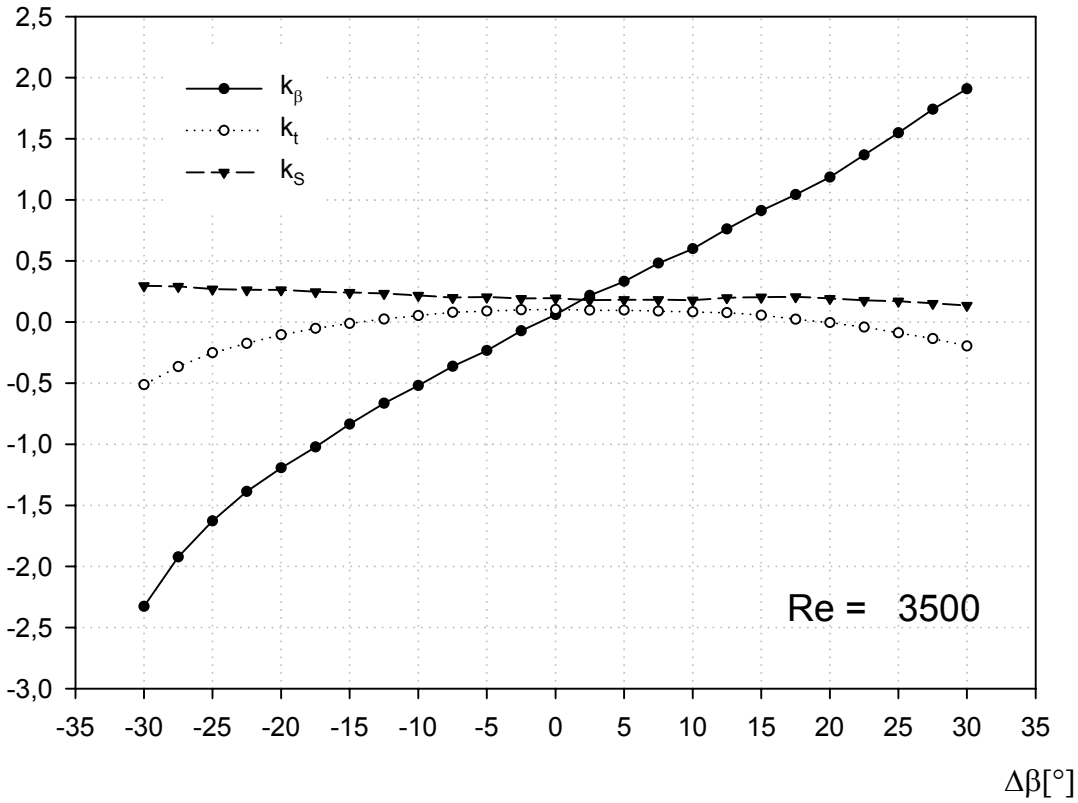

Fig. 11: Calibration coefficients at Re= 3500

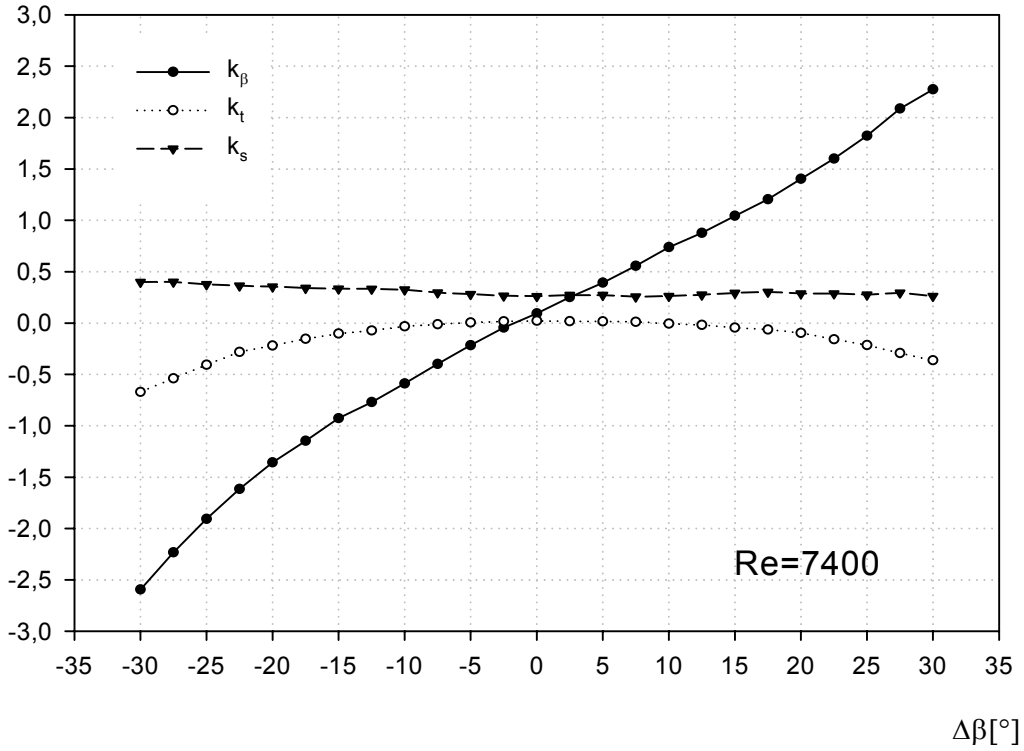

Fig. 12: Calibration coefficients at Re=7400

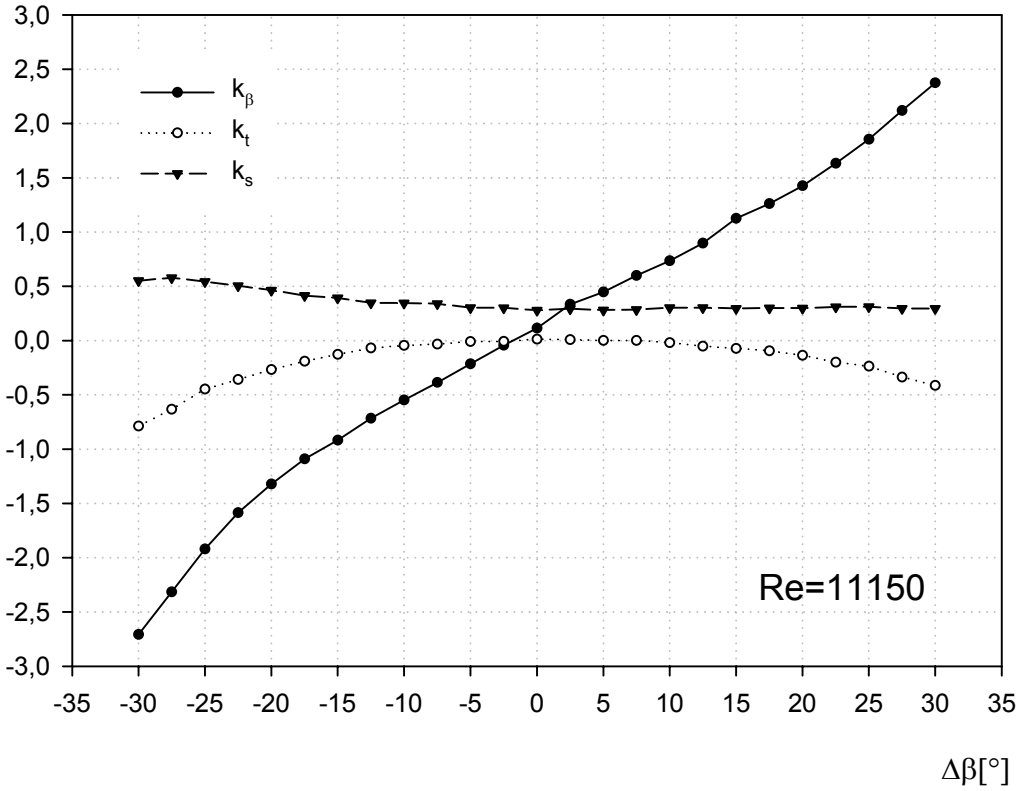

Fig. 13: Calibration coefficients at Re=11150

The hole coefficients k_1, k_2, and k_3 for the three Reynolds numbers (Re=3500, 7400 and 11150) are presented in Fig. 14 to Fig. 16. The hole coefficients are plotted versus the relative flow angle $\Delta\beta$ and can be compared with the value obtained from the streamline projection method (Fig. 4). The distribution of k1 compares well with the theoretical curve. However, the maximum value of k_1 is shifted to about $\Delta\beta$=2°. This indicates that the front face of the three-hole probe under investigation is not strictly perpendicular to the axis of the probe head. The curves for k_2 and k_3 are symmetrical with respect to $\Delta\beta$ =0. This is only true for the theoretical curve. The intersection of k_1 and k_2 of the measured hole coefficients is shifted to $\Delta\beta \approx 2°$.

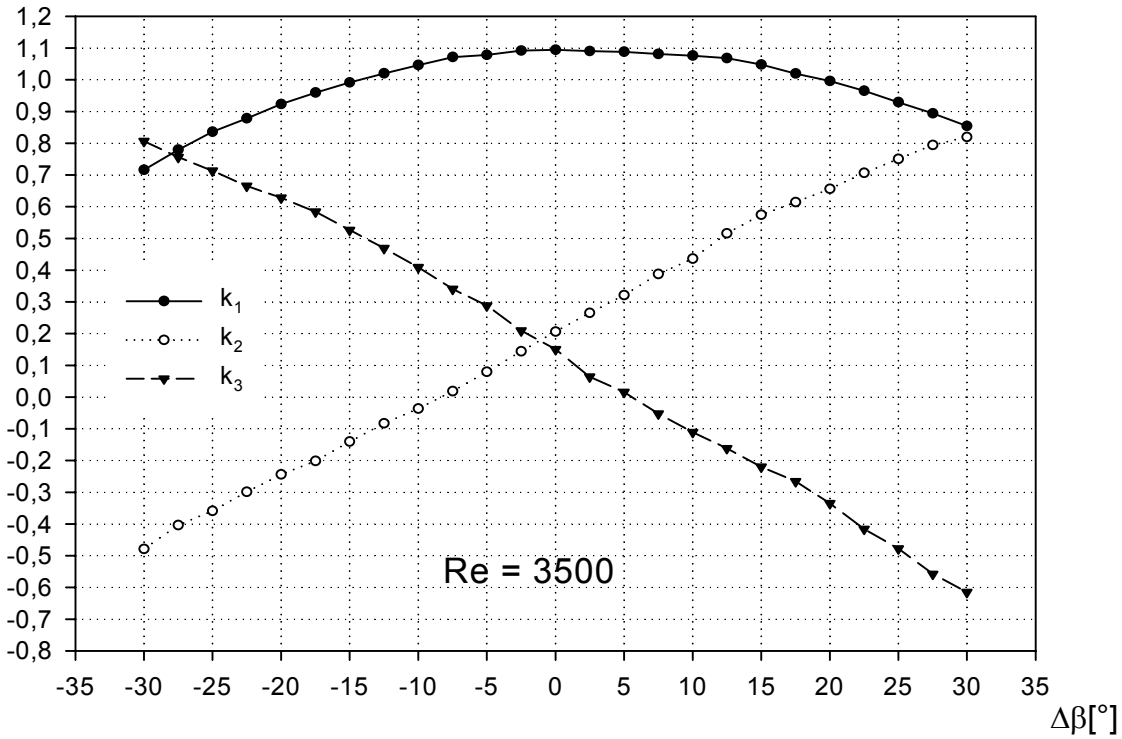

Fig. 14: Hole coefficients at Re=3500

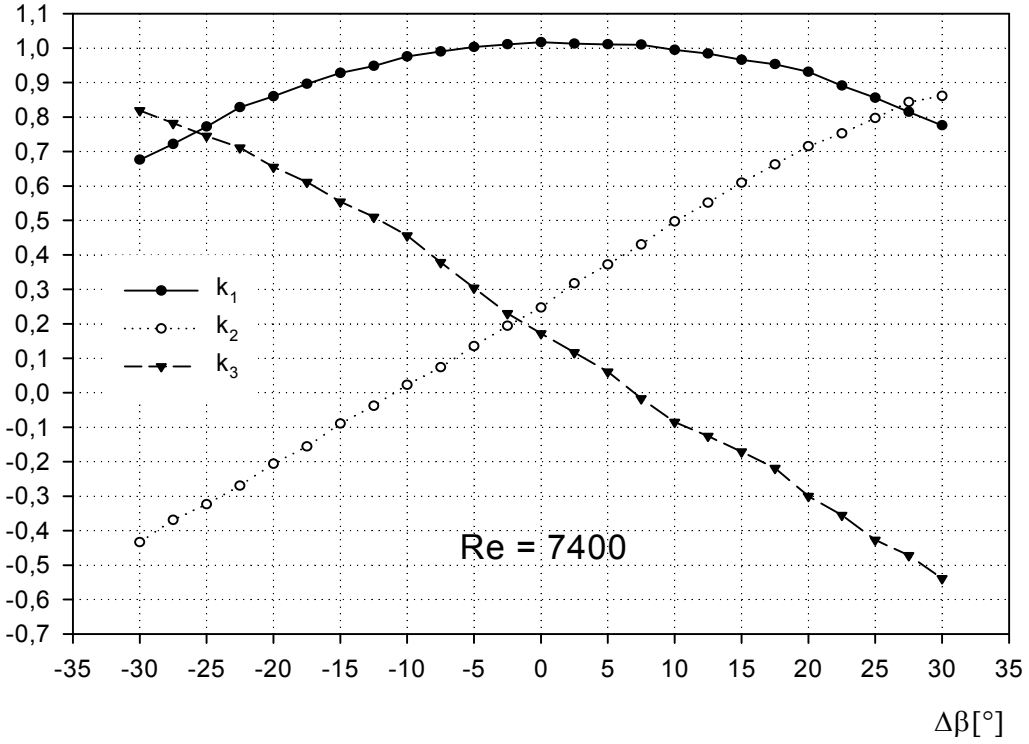

Fig. 15: Hole coefficient at Re=7400

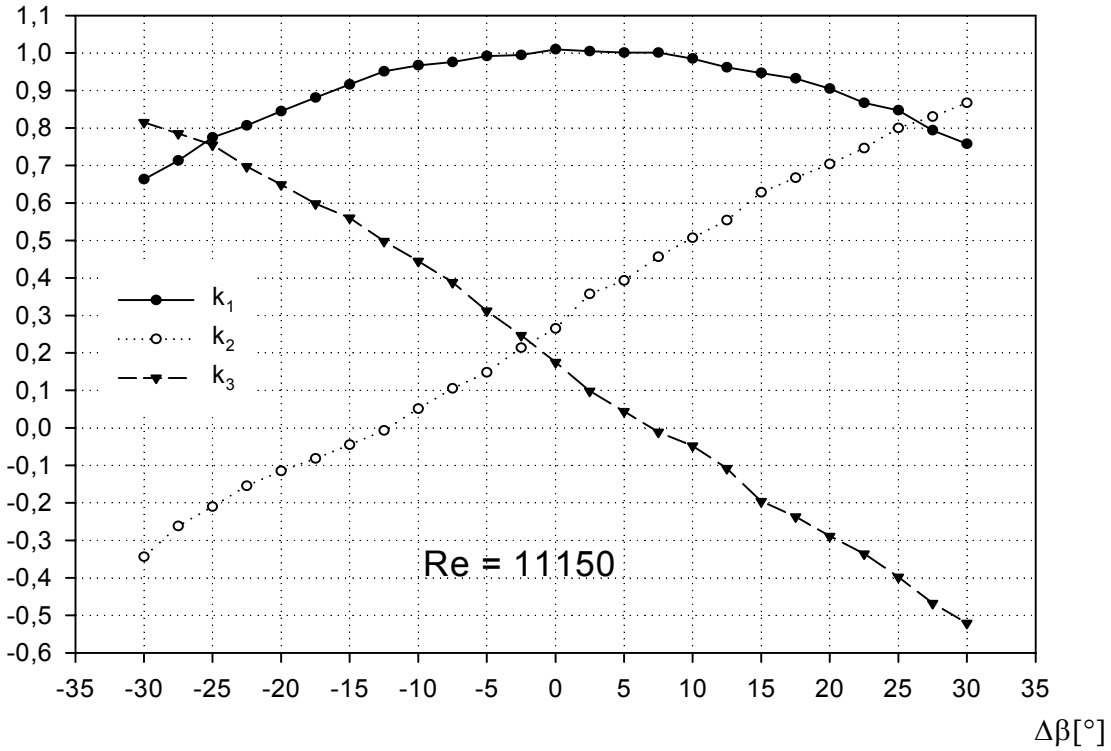

Fig. 16: Hole coefficients at Re=11150

This means that the wedge angle δ=30° is not correctly realized at the three-hole probe under investigation. This corresponds to a visual observation of the probe head. It seems that the wedge angle is slightly higher at the hole 2 and slightly lower at the hole 3, respectively. Due to manufacturing inaccuracies, the theoretical hole coefficients do not match the measured distribution correctly. Another great discrepancy occurs at the suction side of the probe head. This is the flow with hole 3 at $\Delta\beta > 0$ and with hole 2 at $\Delta\beta<0$, respectively. It is expected that the reason for the difference is a flow separation of the section side. Due to the abrupt change in the contour, the flow separates even at low relative flow angles $\Delta\beta$. This separation is of course not modelled by the simple streamline projection method.

10 Results of Calibration with Velocity Gradient

This chapter present the results of the investigation of the influence of the velocity gradient on the behaviour of the three-hole probe. Figure 17 shows the velocity distribution in the boundary layer. This velocity distribution is measured with the 55P15 DANTEC hot-wire probe. The velocity rises in the boundary layer and reaches a free stream value of about 50 m/s. It is difficult to give an exact thickness of the boundary layer. Following Fig. 17, a boundary layer thickness of about 35 mm can be observed.

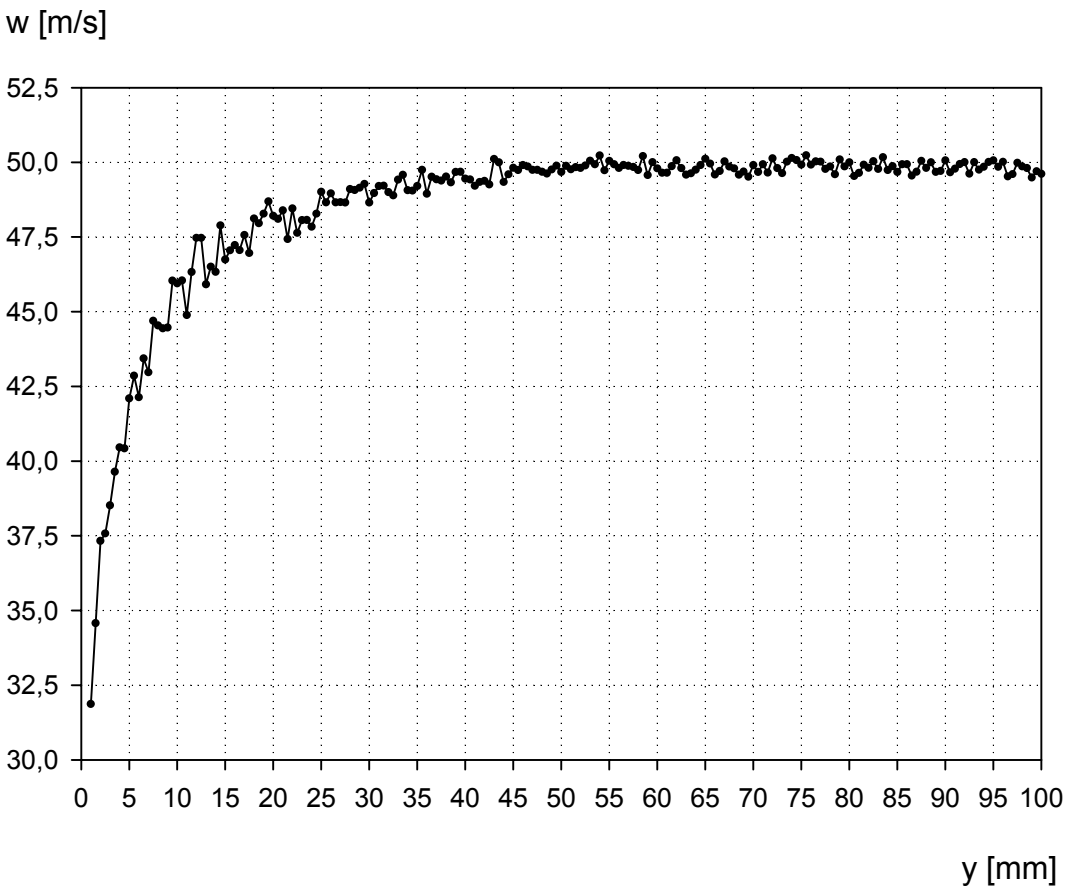

Fig. 17: Velocity distribution in the boundary layer

Not only the distribution of the time averaged velocity but also the turbulence is influenced by the near wall effects. Figure 18 shows the distribution of the streamwise turbulence intensity

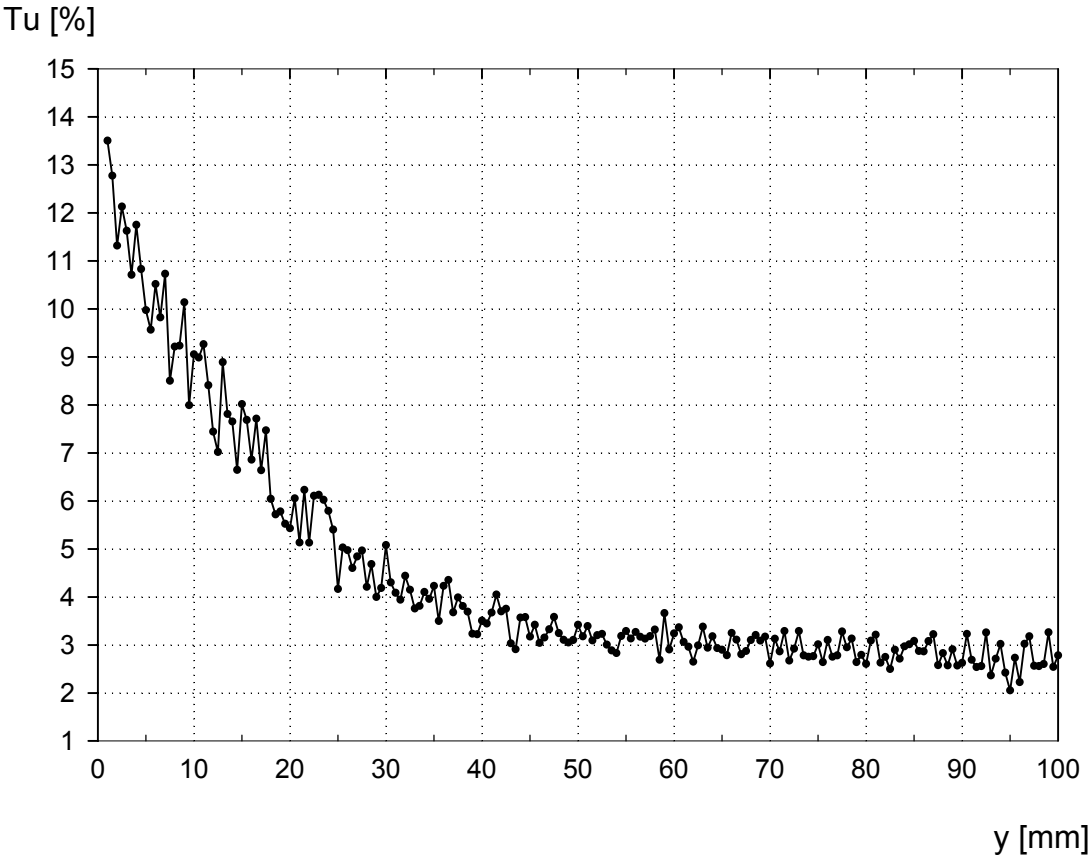

Fig. 18: Turbulence intensity

$$Tu = \frac{\sqrt{\overline{w`^2}}}{w} .$$

Equ. 53

The turbulence in the free stream is about 3% and it rises to about 13% near the wall. When the three-hole probe is traversed perpendicular to the wall through the boundary layer it experiences a velocity gradient.

As a secondary effect, the turbulence intensity also varies when the three-hole probe is traversed through the boundary layer.

As can be seen from Fig. 17, the velocity distribution is not smooth. It showns some fluctuations due to turbulence effects, which especially is true for the flow in the boundary layer. Therefore, it has been decided to make an approximation of the

velocity distribution in the boundary layer. This approximation is based on the power law.

$$\frac{w}{w_\infty} = \left(\frac{y}{\eta}\right)^{1/n}$$

Equ. 54

Figure 19 shows the measured velocity distribution as well an the power law distribution with η=30 mm, w_∞= 50 m/s and n=10. Since only the velocity gradient in the boundary layer is of interest, this distribution is plotted in Fig. 20 Due to various secondary effects not the whole boundary layer thickness can be used for the investigation of the velocity gradient.

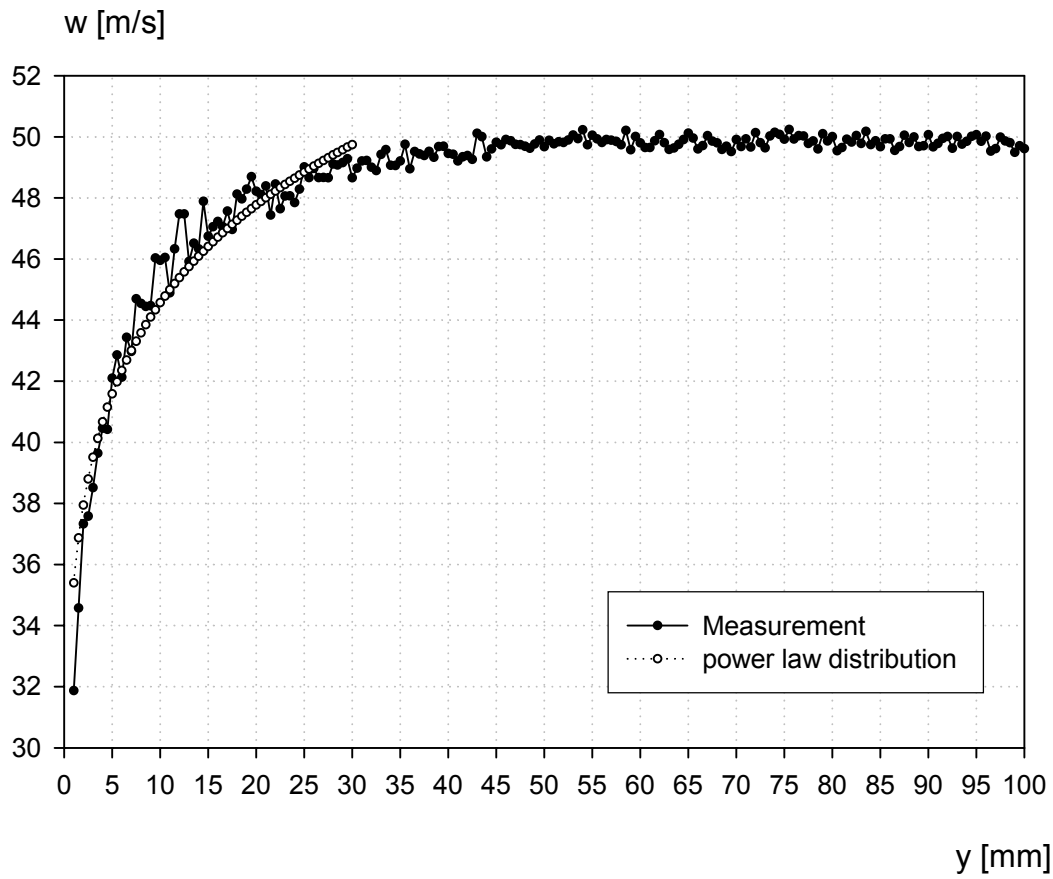

Fig. 19: Velocity distribution with power law

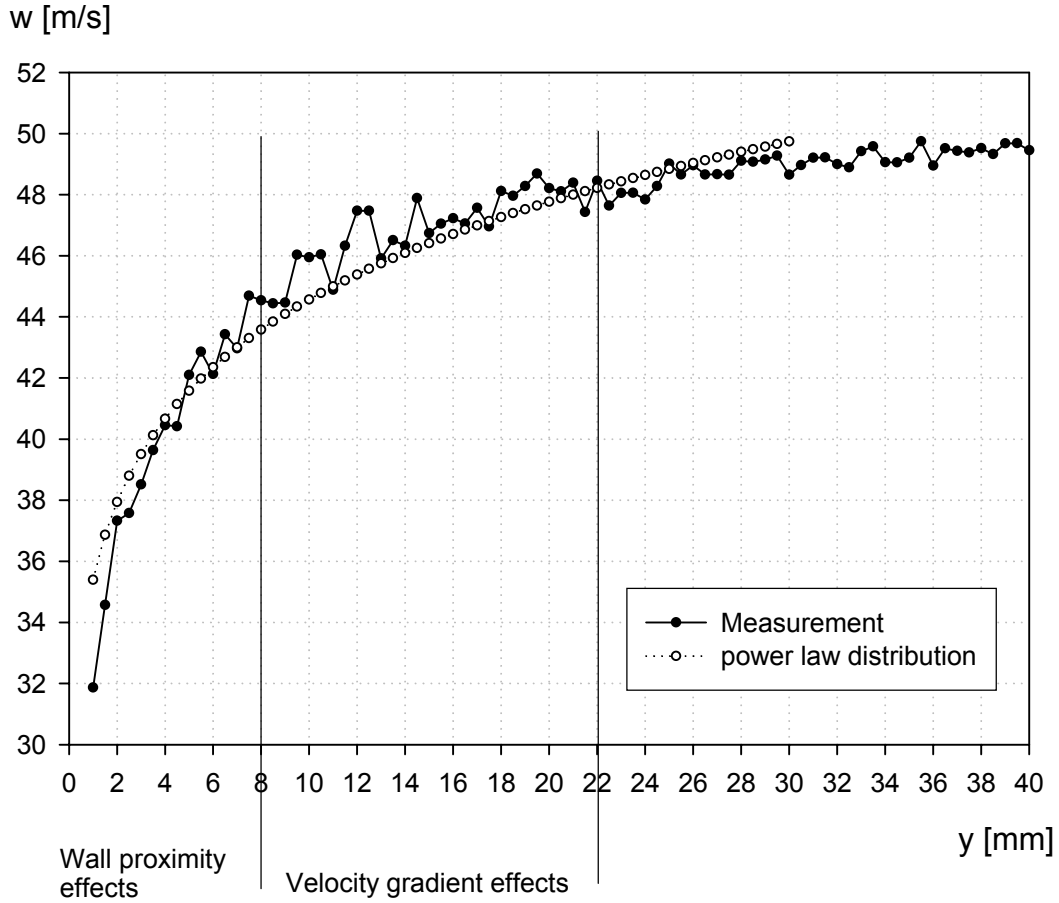

Fig. 20: Velocity distribution and power law inside the boundary layer

As has been shown by Bubeck [1], the wall proximity effects near the solid wall cover a range of about three times the thickness of the pneumatic pressure probe. Due to the blockage effect between the wall and the probe, the pressure in the side hole near the end wall increases compared with the situation in a free stream. Since the thicknes of the three-hole probe under investigation is d=2,4 mm, the region between the wall and y=8 mm can not be used due to wall proximity effects. On the other hand, if y increases the velocity gradient decreases and the gradient effect on the three-hole probe diminishes. Therefore, it has been decided to use only the velocity distribution in the range 8 mm $\leq y \leq$ 22 mm (see Fig. 20)

The nondimensional velocity gradient

$$K = \frac{2 \cdot a_{23}}{w} \frac{dw}{dy}$$

Equ. 55

can be calculated with the imposed power law distribution :

$$\frac{w}{w_\infty} = \left(\frac{y}{\eta} \right)^{1/n}$$

Equ. 56

Since

$$\frac{1}{w} \cdot \frac{dw}{dy} = \frac{1}{ny},$$

Equ. 57

it follows for the nondimensional velocity gradient

$$K = \frac{2 \cdot a_{23}}{n \cdot y}.$$

Equ. 58

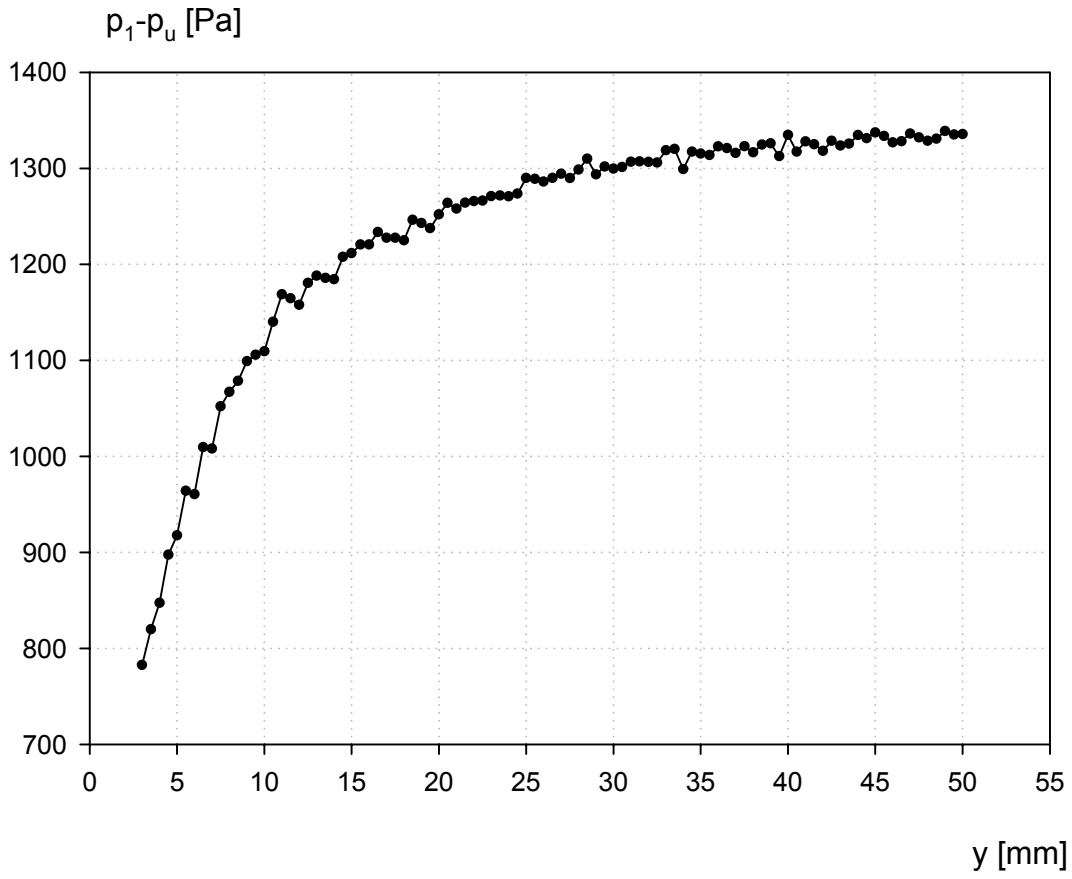

Fig. 21: Measured pressure difference p_1-p_u

The pressure difference between the three holes of the probe and the ambient pressure are ploted in Fig. 21 and Fig. 22, respectively. The distribution of the difference p_1-p_u reflects the influence of the boundary layer on the total pressure. The difference p_2-p_3 in Fig. 22 is a measure for the flow angle error induced by the velocity gradient in the boundary layer. Using the calibration coefficient k_β of the probe in constant velocity (Fig. 12) distributions of $k_\beta(y)$ in Fig. 23 and $\beta(y)$ in Fig. 24 can be derived. The flow angle β in Fig. 24 is induced by the velocity gradient and can be interpreted as the flow angle error. Ideally, the flow is parallel to the wall and therefore β=0.

Using Eq. 58, the wall distance y can be related directly to the nondimensional velocity gradient K. Therefore, the flow angle β versus K is plotted in Fig. 25. The

boundaries of the usefull range of the boundary layer are related to values of K according to the next table.

y [mm]	K [-]
8	0,0400
22	0,0145

As can be seen from Fig. 25, the distribution of β flattens for K<0,04. This effect is caused by the wall proximity. Figure 26 shows the distribution of the induced flow angle β in the range 0,04 $\geq K \geq$ 0,015. This distribution is approximated by a linear curve according to the least square method

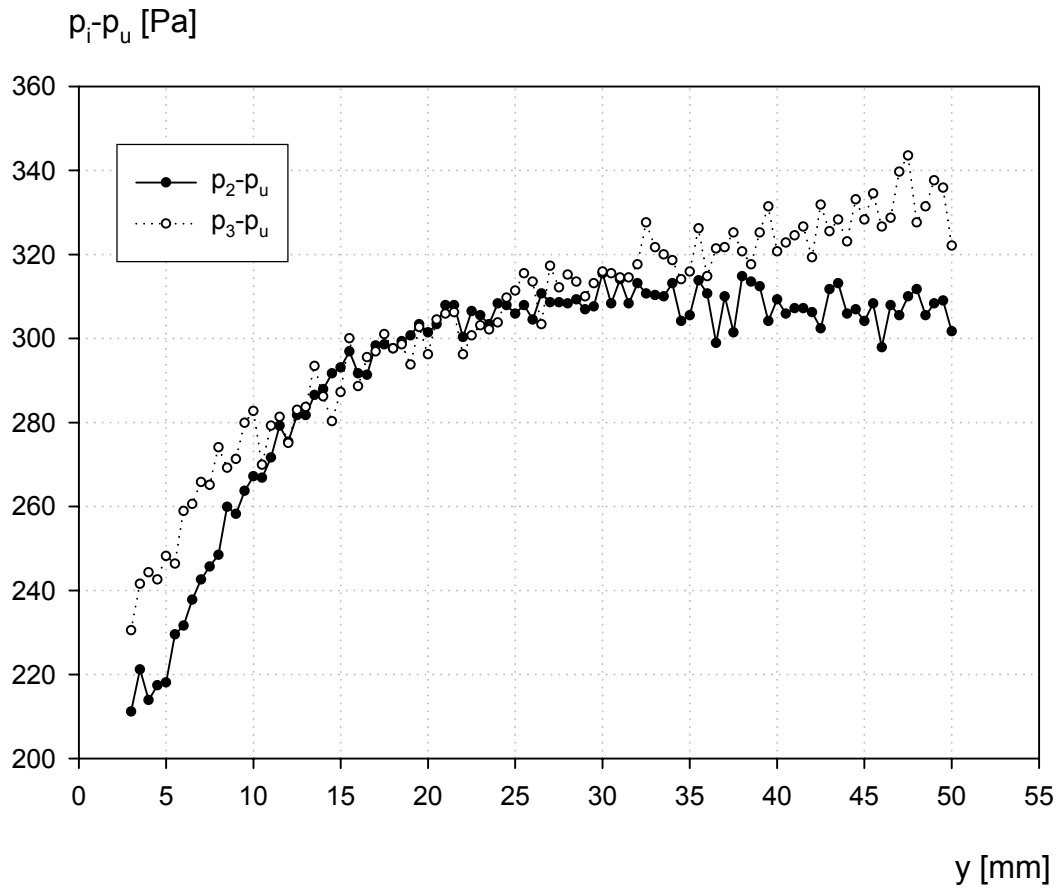

Fig. 22: Measured pressure differences p_2-p_u and p_3-p_u

$$\beta = 16{,}49 \cdot K - 1{,}23$$

Equ. 59

The slope of this linear distribution can be interpreted as the coefficient C in the equation of the flow angle error:

$$\Delta\varepsilon = C \cdot K = 16{,}49K$$

Equ. 60

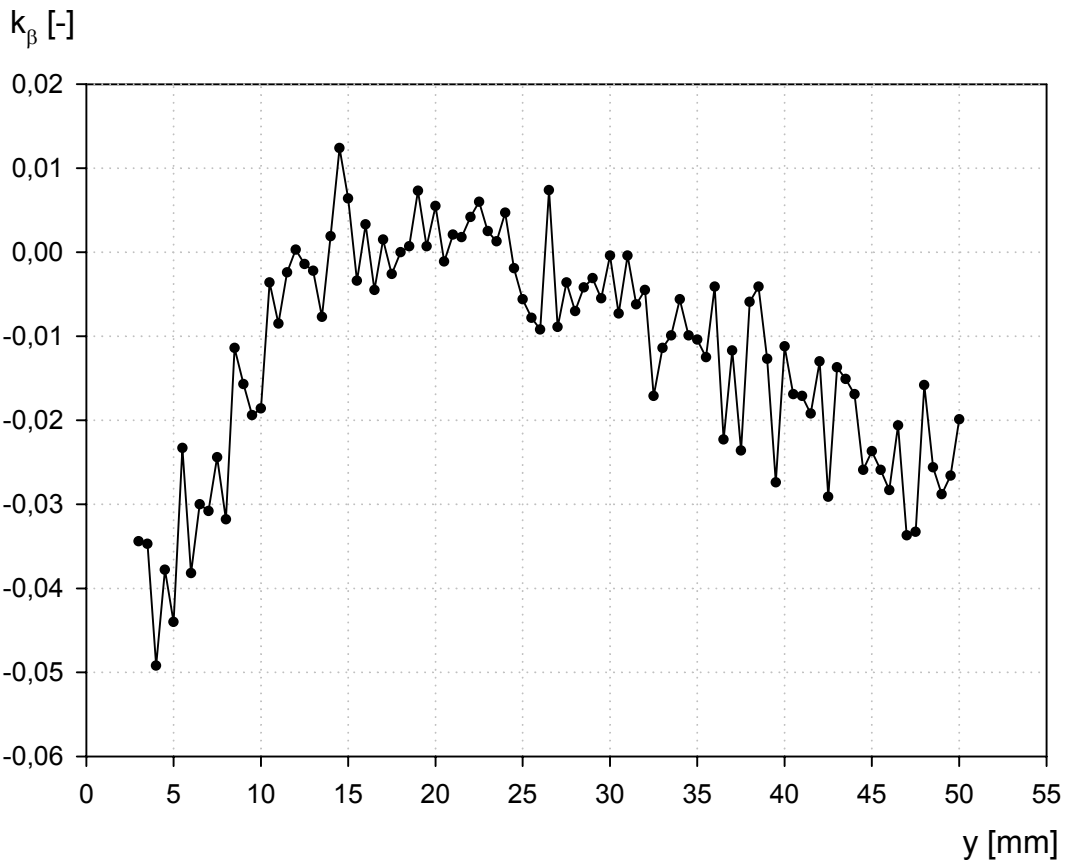

Fig. 23: Distribution of the directional coefficient k_β in the boundary layer

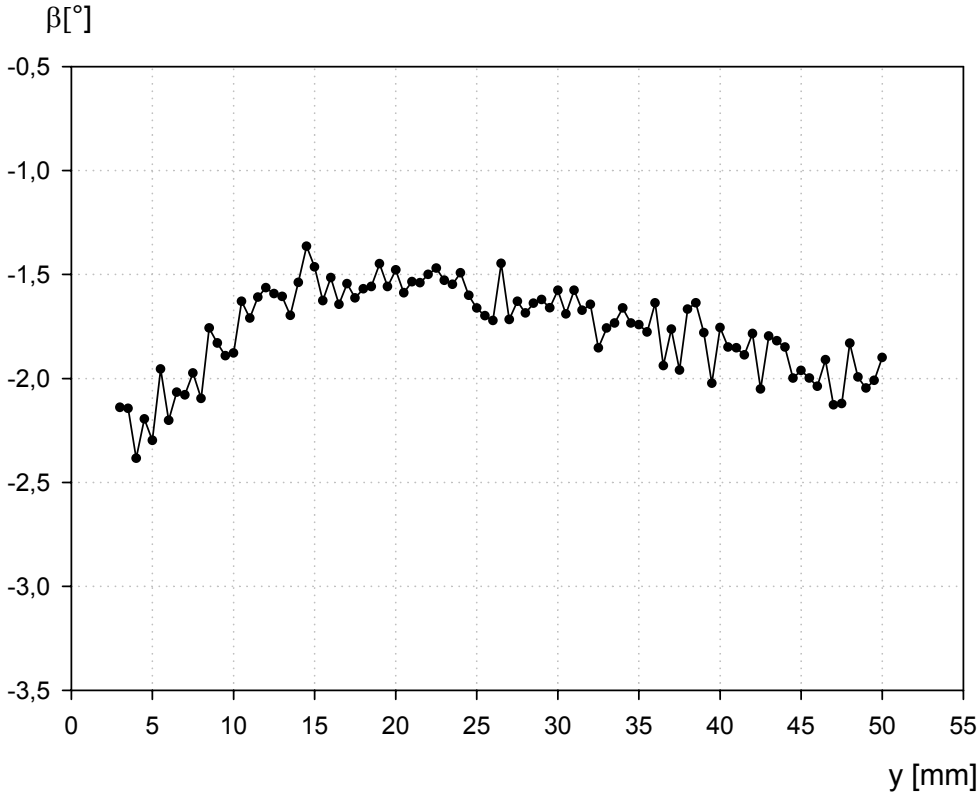

Fig. 24: Distribution of the induced flow angle β in the boundary layer

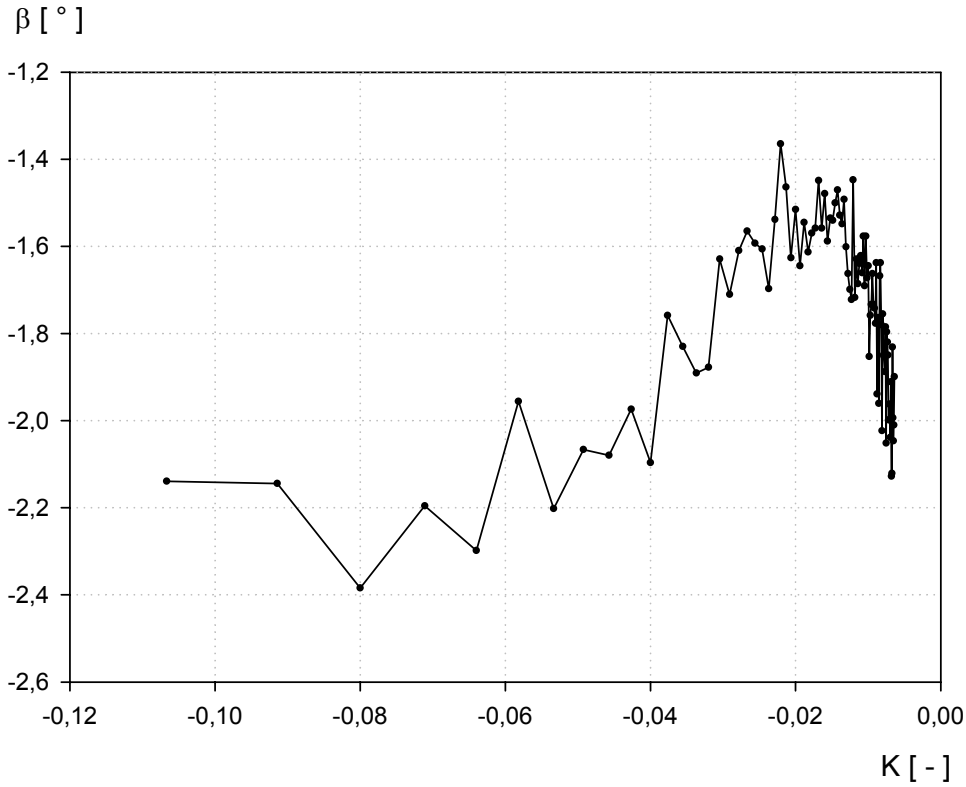

Fig. 25: Distribution of the flow angle β versus the nondimensional velocity gradient K

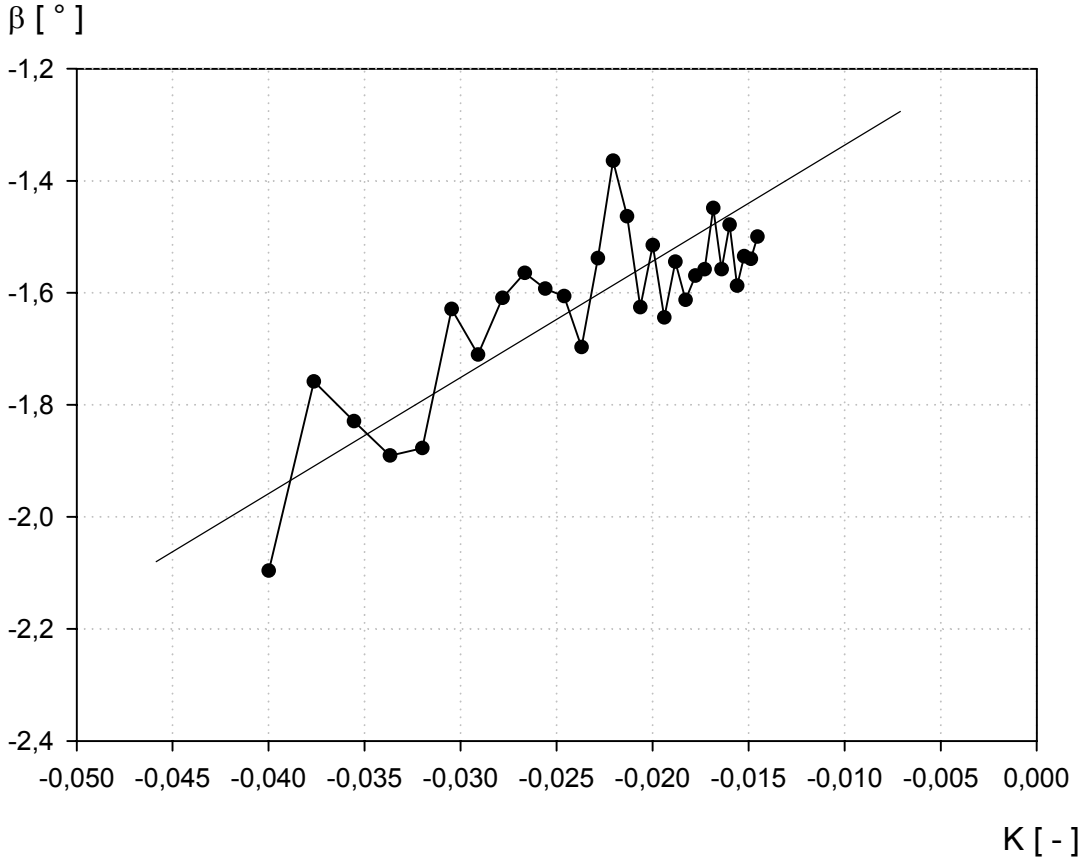

Fig. 26: Linear approximation of the flow angle β versus the nondimensional velocity gradient K

11 Application of the Velocity Gradient Correction

In this chapter, the correction method for the flow angle error induced by the velocity gradient is applied to the measurement downstream of a linear turbine cascade. The cascade with high flow corresponds to the high pressure blading of an industrial steam turbine. The three-hole probe is traversed over one pitch about 8% axial chord lengths downstream of the cascade exit plane Since the two-dimensional flow is of interest, the probe is traversed at half span.

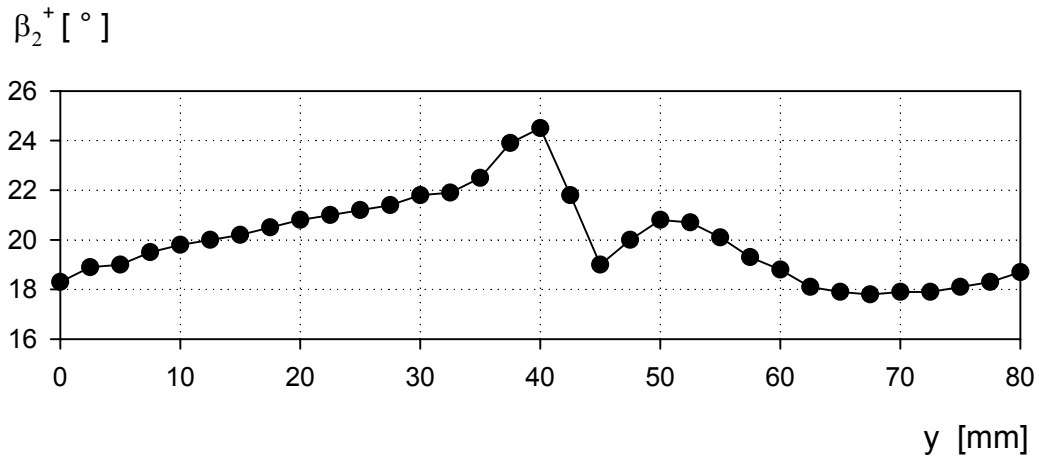

Fig. 27: Measured flow angle s downstream of the linear turbine cascade (without correction)

Figure 27 shows the distribution of the measured flow angle β_2^+ without correction. The flow angle varies between 18° and 22°. However, some over- and undershoot is visible immediately downstream of the turbine blade. The overshoot on the pressure side as well as the undershoot at the section side are induced by the velocity gradient of the blade wake. This can be seen in the velocity distribution in Fig. 28.

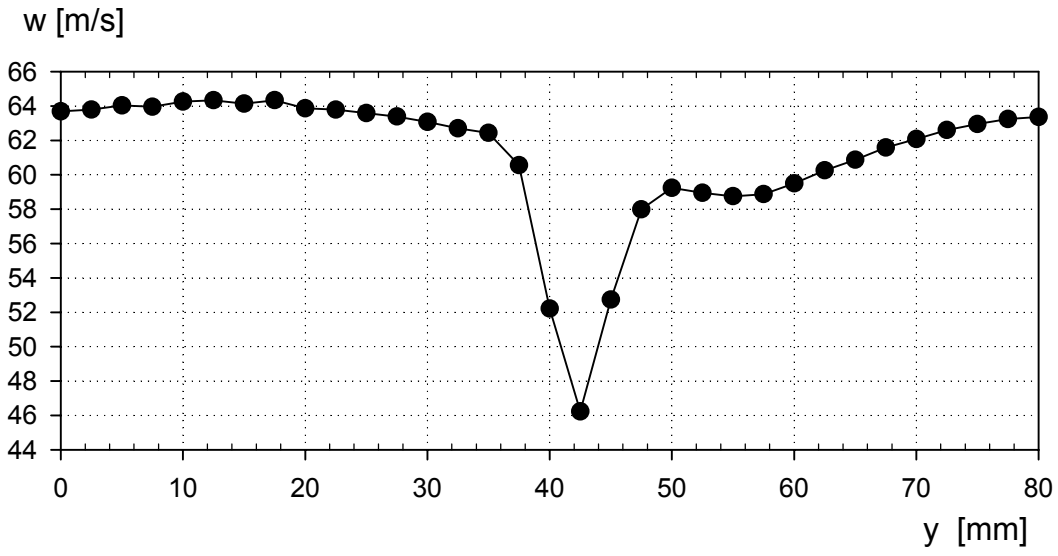

Fig. 28: Measured velocity distribution downstream of the linear turbine cascade

Figure 29 shows the distribution of the nondimensional velocity gradient K obtained from the measured velocities. K is nearly zero in the freestream region. High negative values (K= -0,18) in the pressure side wake and high positive values (K=0,18) in the section side wake can be seen in Fig. 29 Following Eq. 60, the nondimensional velocity gradient K can be transformed to the error of the flow angle $\Delta\varepsilon$. This distribution is plotted in Fig. 29 for C= 16,49.

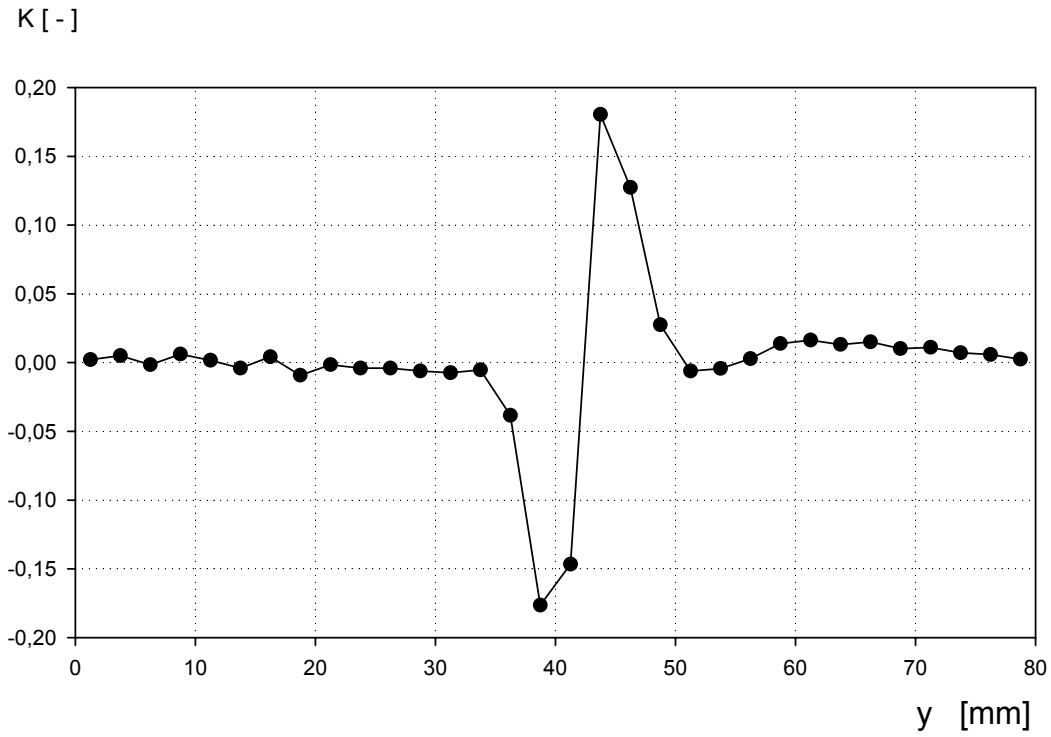

Fig. 29: Nondimensional velocity gradient downstream of the linear turbine cascade

The correction method is applied to the measured flow angles and the result is ploted in in Fig. 31. As can be seen, the flow angle distribution is smoother and the over- as well as the undershoots have been diminished .

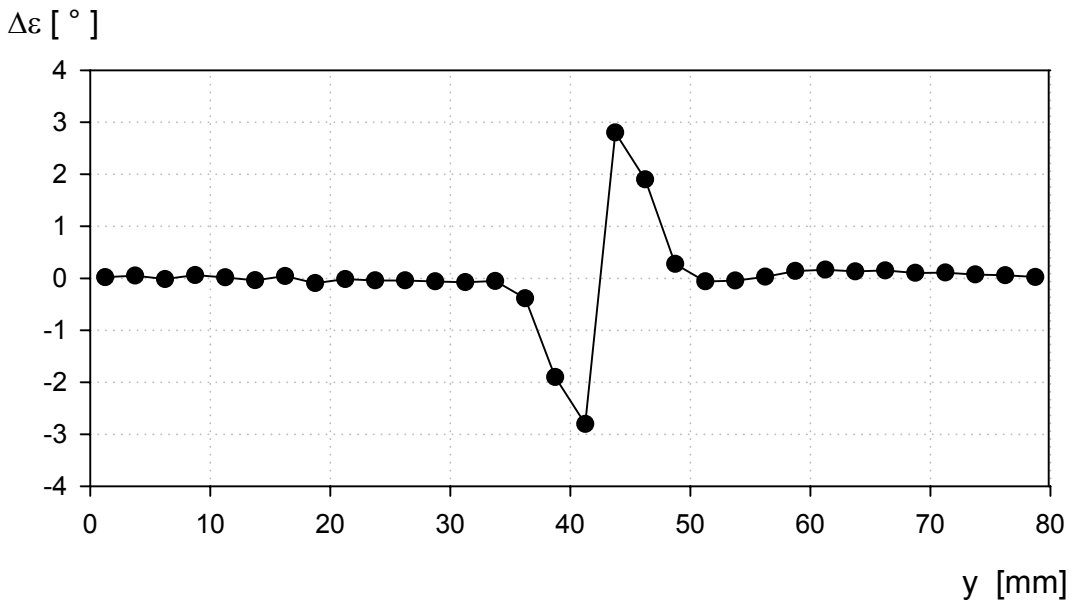

Fig. 30: Correction Δε of the flow angle downstream of the linear turbine cascade

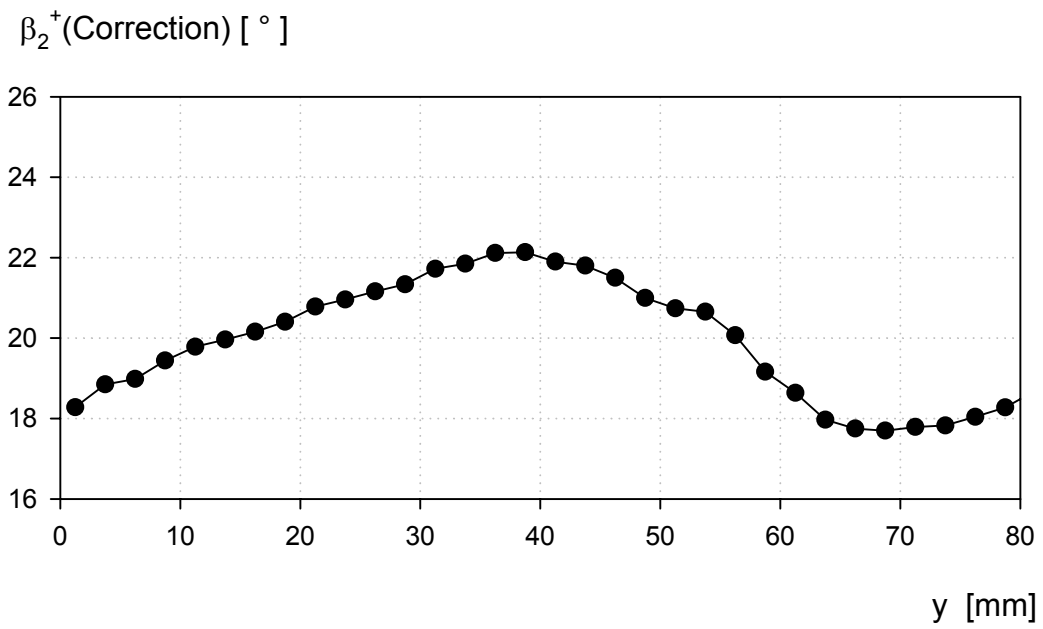

Fig. 31: Measured flow angle downstream of the linear turbine cascade (with correction)

12 Summary and Conclusions

The present work describes an investigation on the effects of velocity gradients on the flow angle error of pneumatic three-hole probes. The flow angle error $\Delta\varepsilon$ depends an the nondimensional velocity gradient K according to:

$$\Delta\varepsilon = C \cdot K$$

Equ. 61

The constant C depends an the geometry of the probe head. A simple analytical investigation based on the streamline projection method gives C= 8,27 for the probe under investigation (wedge angle δ=30°). A literature survey shows different values for the constant C. Ikui and Inoue [5] have been measured C=13,2 for a cobra probe with δ=45°, whereas Dixon [2] states C=16,76 for a wedge probe. The present investigation gives C=16,49 for the-three hole probe. The probe is traversed in a boundary layer with a thickness of about 35 mm. The probe head has a dimension d=2,4 mm and therefore, wall proximity effects are appreciable for $0 \leq y \leq 8$ mm.

This is a disadvantage of the present method. To avoid this, future investigations on gradient effects should be done in a free shear flow (wake).

The correction method is applied to the measured flow downstream of a linear turbine cascade. An appreciable improvement of the measured flow angle in the blade wake region is obtained.

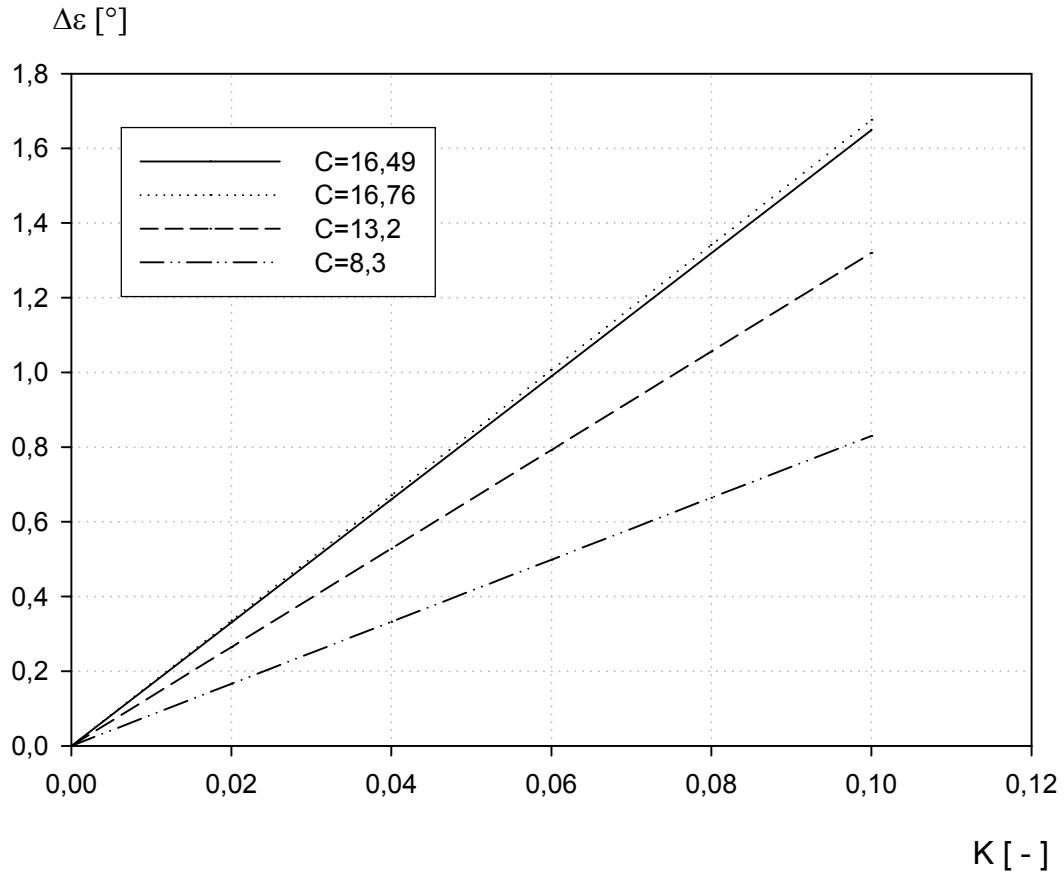

Fig. 32: Summary of the flow angle error Δε versus the nondimensional velocity gradient K

13 Bibliography

[1] Bubeck, H.: Entwicklung einer Keilsonde zu dreidimensionalen instationären Strömungsmessung und deren Anwendung in einem Axialverdichter. Dissertation, Universität Stuttgart (1987)

[2] Dixon S. L.: Measurement of Flow Direction in a Shear Flow. J. Phys E: Sci. Instrument., Vol. 11 (1978)

[3] Dominy R.G., Hodson H.P.: An Investigation of Factors Influencing the Calibration of Five-Hole Probes for Three-Dimensional Flow Measurement. ASME Journal of Turbomachinery ,Vol. 115 (July 1993)

[4] Huffman G. D., Robe D.C., Poti N.D.: Flow Direction Probes From a Theoretical and Experimental Point of View. J. Plhys E: Sci. Instrument., Vol. 13 (1980)

[5] Ikui T., Inoue M.: Pressure or Velocity Gradient Error in the Flow Direction Measurement. Memoirs of the Faculty of Engineering Kyushu University, Vol. 29, No. 3 (March 1970)

[6] Sitaram N., Lakshminarayana B., Ravindranath A.: Conventional Probes for the Relative Flow Measurement in a Turbomachinery Rotor Blade Passage. ASME Journal of Engineering for Power, Vol. 103 (April 1981)

[7] Shepherd I. C.: A Four Hole Pressure Probe for Fluid Flow Measurement in Three Dimensions. ASME Journal of Fluids Engineering, Vol. 103 (December 1981)

[8] Smout P.D., Ivey P.C.: Investigation of Wedge Probe Wall Proximity Effects. Part 1 and Part 2. ASME Journal of Engineering for Gas Turbines and Power Vol. 119, (July 1997)

[9] Smout P. D., Ivey P. C.: Wall Proximity Effects in Pneumatic Measurement of Turbomachinery Flows. ASME paper 94-GT-116 (1994)

[10] Treaster, A.L, Yocum, A.M: The Calibration and Application of Five-hole Probes. ISA Transactions Vol. 18, No.3 (1979)

14 Pictures List